Chemical Geology 598 (2022) 120831

Contents lists available at ScienceDirect

Chemical Geology

journal homepage: www.elsevier.com/locate/chemgeo

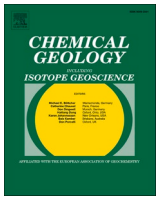

Extending classical geochemical weathering studies through the mountain block: The effect of increasing scale on geochemical evolution in the Sierra Nevada (CA)

Zachary P. Meyers [a,*], Laura K. Rademacher [a], Marty D. Frisbee [b], Sara R. Warix [c]

[a] Department of Geological and Environmental Sciences, University of the Pacific, 3601 Pacific Avenue, Stockton, CA 95211, USA
[b] Department of Earth, Atmospheric, and Planetary Sciences, Purdue University, 550 Stadium Mall Drive, West Lafayette, IN, USA
[c] Hydrologic Sciences and Engineering, Colorado School of Mines, 1500 Illinois St, Golden, CO 80401, USA

ARTICLE INFO

Editor: Karen Johannesson

Keywords:
Geochemical evolution
Mountain front springs
Granite weathering
Sierra Nevada
Excess calcium

ABSTRACT

The seminal studies of Feth et al. (1964) and Garrels and Mackenzie (1967) describe the chemical weathering processes controlling the geochemistry of spring waters in the Sierra Nevada (CA) and provide a framework for understanding geochemical weathering processes at local groundwater scales (i.e., short distances between recharge and subsequent groundwater discharge). Here, we extend these concepts to investigate the factors controlling geochemical evolution at the intermediate, mountain-block scale (i.e., increased flowpath length, circulation depth, and rock-water interaction). We accomplish this by applying a multi-tracer approach to mountain-front springs emerging along the Sierra Nevada frontal fault zone in Owens Valley, CA. These springs emerge at a significantly lower elevation (1100–2000 mamsl) than the eastern Sierra crest (4000+ mamsl) and provide a window into the hydrogeological and hydrochemical processes occurring within the mountain block from high-elevation mountain-block recharge to low-elevation mountain-front discharge, a recognized knowledge gap in hydrogeology. We delineate approximate spring contributing areas and identify geologic units likely sourcing springflow using stable isotopes of water and dissolved noble gases. We then classify four major geochemical groups after identifying the likely geologic units sourcing springflow and subsequent analysis and modeling of spring geochemistry. Our results lead to three main conclusions: 1) geochemical evolution within the mountain block from high elevation mountain block weathering to mountain front discharge follows power-law weathering relationships and becomes increasingly dependent on the dissolution of disseminated calcite present in plutonic rocks with increasing flowpath length, 2) geologic heterogeneity (i.e., differences in plutonic compositions and the presence/absence of Paleozoic metasedimentary roof pendants) exerts a dominant control on geochemical evolution with increased flowpath length, and 3) within geochemical groups, simple metrics like TDS or mole transfers from inverse geochemical models scale with physical and isotopic indicators of groundwater circulation and flowpath length.

1. Introduction

Chemical evolution of springs in the Sierra Nevada, CA, USA is the basis for two classic contributions in the field of water chemistry: Feth et al. (1964) and Garrels and Mackenzie (1967). These seminal works provide a framework for interpreting groundwater geochemical evolution from precipitation to ephemeral springs and to perennial springs through establishment of a conceptual model that ties groundwater chemistry to aquifer mineralogy. An underlying tenet within Garrels and Mackenzie (1967) is that groundwater ion concentrations derived from rock-water interaction will scale with distance from recharge, and thus, flowpath length and groundwater circulation depth. These relationships are critical to understanding how weathering and geochemistry evolve with increasing flowpath length beyond local-scale shallow groundwater to intermediate (i.e., mountain block) and regional (i.e., aquifer and basin) scales.

Just as Garrels and Mackenzie (1967) built upon the work by Feth et al. (1964) in improving our understanding of the controls on aqueous

* Corresponding author.
E-mail addresses: zmeyers1@pacific.edu (Z.P. Meyers), lrademacher@pacific.edu (L.K. Rademacher), mdfrisbee@purdue.edu (M.D. Frisbee), swarix@mines.edu (S.R. Warix).

https://doi.org/10.1016/j.chemgeo.2022.120831
Received 6 January 2022; Received in revised form 17 March 2022; Accepted 23 March 2022
Available online 26 March 2022

geochemistry in a well-studied granitic terrain, a number of other well-cited geochemical studies followed and improved our understanding of the Sierra Nevada, making it one of the best studied mountain ranges, hydrologically and geochemically, in the United States. Studies in the Sierra Nevada have examined 1) chemical evolution in shallow groundwater (Feth et al., 1964; Garrels and Mackenzie, 1967; Rademacher et al., 2001), 2) small catchment-scale geochemical evolution (Williams and Melack, 1991; Holloway and Dahlgren, 2001; Rademacher et al., 2001; Rademacher et al., 2005) 3) sources of solutes in streamflow (Blum et al., 1993; Pretti and Stewart, 2002), and 4) regional evolution from the mountain block into alluvium and alluvial basins (Güler and Thyne, 2004a; Güler and Thyne, 2004b; Guler and Thyne, 2006). Feth et al. (1964) and other studies in the area (e.g., Rademacher et al., 2001) previously observed a linear trend for geochemical evolution within the Sierra Nevada at local spatial scales (e.g., Fig. 1A). However, there still exists a knowledge gap regarding the processes controlling rock-water interaction and geochemical evolution at depth in the mountain block, i.e., groundwater flowing at intermediate scales prior to chemical overprinting by alluvial basin material (Fig. 1B). While hillslope and catchment-scale groundwater flow studies are useful in understanding hydrogeochemical processes at limited spatial scales following recharge, findings from these studies may not apply to areas where deeper/older groundwater may dominate baseflow or springflow (e.g., Frisbee et al., 2011). On the other hand, regional studies (e.g., Güler and Thyne, 2004a, 2004b) principally focus on geochemical evolution derived from highly soluble evaporites and alluvial basin fill, thus overlooking the complexity of geochemical processes occurring between initial recharge and the mountain front (Dreher, 2003).

Recent research confirms that the circulation of groundwater in the mountain block bedrock is an important contributor to mountain streamflow and lowland aquifers (Hayashi, 2020; Markovich et al., 2019; Somers and McKenzie, 2020). However, mountain-block groundwater remains one of the least understood components of the hydrologic cycle (Gardner et al., 2018). In particular, the chemical evolution that occurs during deeper groundwater circulation and alters the kinetics of watershed solute weathering fluxes remain unclear.

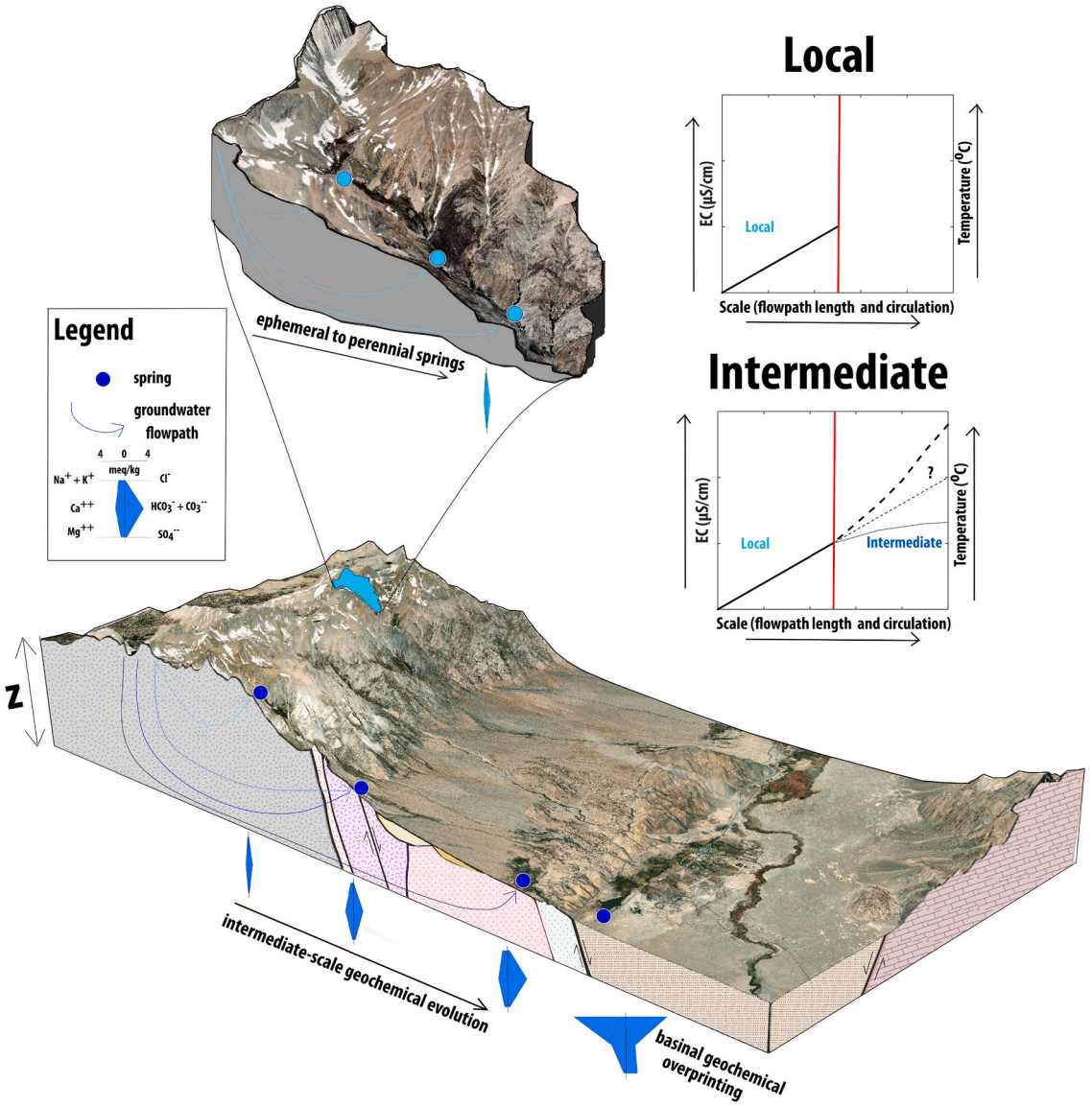

Fig. 1. Conceptual model for geochemical evolution at intermediate scales as a function of flowpath length and circulation as shown by Stiff diagrams of mountain block and mountain front springs. Within the conceptual model, inset graphs show the relationships among scale, temperature, and EC. The red line represents the division between "Local" scale and "Intermediate" scale. (For interpretation of the references to colour in this figure legend, the reader is referred to the web version of this article.)

Capturing this intermediate-scale, mountain block flow component is difficult, as bedrock wells are expensive and few in number (Manning and Solomon, 2005). However, perennial springs emerging at the mountain front provide an alternative window into mountain block groundwater processes (Manning and Solomon, 2003; Wilson and Guan, 2004). For example, many springs emerge in Owens Valley, CA at the Sierra Nevada frontal fault zone along the eastern escarpment of the Sierra Nevada. These springs are representative of intermediate-scale groundwater flow as they emerge at a significantly lower elevation (1000–2000 mamsl) than their likely recharge areas (2600–4000+ mamsl) in talus and fractured bedrock above the tree line. Therefore, these springs provide a means to naturally extend the work of Feth et al. (1964) and Garrels and Mackenzie (1967) from local-scale flowpaths to intermediate-scale flowpaths (e.g., Fig. 1B). While the volumetric significance of water recharging through the fractured plutonic mountain block into the Owens Valley basin fill aquifer may be limited (Danskin, 1998), these aridland mountain front springs support groundwater dependent ecosystems that are keystone features and biodiversity

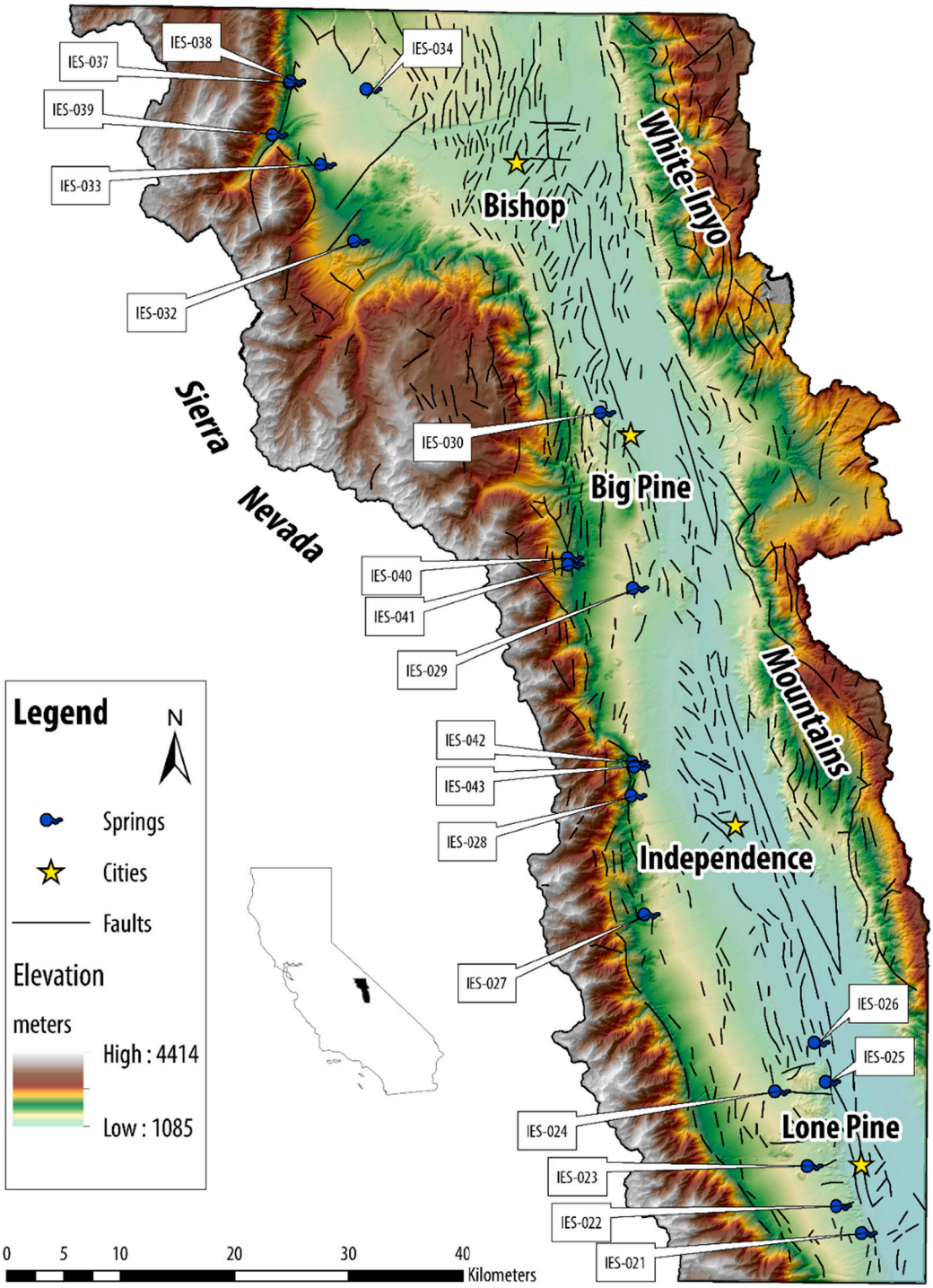

Fig. 2. Map showing locations and sample IDs (IES-###) of sampled study springs in Owens Valley, CA within the Crowley Lake and Owens Lake watersheds. Eastern and western map boundaries correspond to watershed divides. Map outline location within California is highlighted on the inset map. Elevation data for the study area were acquired from The National Map (TNM), a part of the USGS National Geospatial Program.

hotspots for aquatic (Sada and Herbst, 2001; Sada, 2008) and terrestrial species (Conroy et al., 2016; Patton and Conroy, 2017).

In this study we use multiple geochemical and isotopic diagnostic tools to delineate groundwater flowpaths and provide insight into the processes that control geochemical evolution at the mountain-block scale by investigating mountain front springs in Owens Valley, CA (Fig. 2). We seek to answer the following questions: 1) How do increasing groundwater flowpath length and circulation depth influence spring geochemical composition from local to intermediate spatial scales? 2) What are the rough contributing areas of recharge and the geologic units contributing flow for mountain front springs? and 3) What are the dominant controls on geochemical evolution with increasing flowpath length?

2. Study area

2.1. Regional geography

The Mono-Owens Lake Watershed is an internally drained watershed in eastern California (HUC 180901) that comprises the Mono Lake Watershed, the Crowley Lake Watershed, and the Owens Lake Watershed. This study focuses on the Crowley Lake and Owens Lake portions of HUC 180901 (Fig. 2). These watersheds are bounded by the eastern Sierra Nevada to the west and the White-Inyo Mountains to the east. Moving south across the Volcanic Tableland, elevation decreases significantly from Crowley Lake (2065 mamsl) to Bishop, CA (1267 mamsl) over a distance of 40 km. From Bishop to the terminus of the Owens River south of Lone Pine, the elevation change is more gradual, with a net change of ~185 m over 108 km.

2.2. Climate and precipitation

Owens Valley lies in the rain shadow of the Sierra Nevada and averages 13.4 cm of precipitation annually, the majority of which falls as rain in the valley (NOAA Station: Bishop, CA). At the northern end of the valley (i.e., Bishop, CA), the average annual high temperature is 23.6 °C and the average annual low temperature is 3.1 °C. At higher elevations in the eastern Sierra Nevada, precipitation usually falls as snow and annual amounts are highly variable due to the effects of local topography (Elder et al., 1989; Zheng et al., 2016). High-elevation locations in the surrounding mountains average over 250 cm of total snowfall annually. Alpine areas in the eastern Sierra have average annual high temperatures of 10 to 13 °C and average annual low temperatures of −2.5 to −3 °C (NOAA Stations: South Lake, CA and Lake Sabrina, CA).

2.3. Hydrology

Snowmelt from the Sierra Nevada and White-Inyo Mountains supports surface-runoff and streamflow into Owens Valley, and it is also the principal source of recharge for both the mountain-block and basin-fill aquifers (Danskin, 1988; Danskin, 1998). In the basin, surface-water flow initiates primarily from snowmelt runoff in the northern part of the watershed in Mono County before flowing southward via an axial drainage system (the Owens River) and terminating in the now dry Owens Lake. Perennial streams drain the ranges on both sides of the valley, however a far greater number of tributaries to the Owens River emerge from the western side of the valley as the White-Inyo Mountains are in a prevailing rain-shadow and receive significantly less precipitation. Both the surface water and groundwater systems in Owens Valley have been significantly altered by construction of the Los Angeles Aqueduct (LAA) and subsequent projects resulting in the diversion of water out of the valley. The LAA altered the hydrology and thus the economic development of Owens Valley by diverting water from the Owens River and pumping groundwater from the basin aquifer during dry years (Kahrl, 1976). The development of the LAA, combined with irrigation withdrawals in the valley, ultimately led to the desiccation of Owens Lake, an endorheic basin lake just south of Lone Pine, CA (Reheis, 1997). Groundwater recharge via precipitation at lower elevations in the basin is minimal (Danskin, 1998).

Numerous perennial springs emerge along the mountain front of the eastern Sierra Nevada and are often associated with zones of faulting (strike slip and normal) (Danskin, 1988; Hollett et al., 1991; Danskin, 1998). The mountain-front springs emerge at elevations higher than the valley floor, and flow from these springs is therefore not impacted by irrigation or diversions in the valley. We sampled a subset of these springs (Fig. 2) during the spring of 2016 to capture: 1) a broad spatial distribution, 2) the geologic heterogeneity of the batholith, and 3) to address questions about geochemical evolution with increasing scale from high elevation mountain block recharge to mountain front spring discharge. The majority of sampled springs are pristine rheocrenes (i.e., springs that form small streams) with spring brooks that eventually infiltrate into pluton-derived alluvial material.

2.4. Geology

Structurally, Owens Valley is a rift basin with over 3000 m of basin fill lying just outside the Basin and Range physiographic province in what is known as the Walker Lane (Wesnousky, 2005; Jayko and Bursik, 2011). This tectonic setting creates a significant amount of relief where Owens Valley (~1000–1400 mamsl) is surrounded on both sides by north-south trending ranges with ridgelines and peaks exceeding 4000 mamsl. Faulting in the area is pervasive due to the complex tectonic history. There are many small transform faults associated with strike-slip displacement from the Walker Lane, locally known as the Eastern California Shear Zone (ECSZ) (Wesnousky, 2005; Jayko and Bursik, 2011), as well as numerous normal and detachment faults associated with Basin and Range extension (Taylor and Dewey, 2009). As shown in Fig. 2, these faults are prevalent throughout the basin and are often related to areas of groundwater discharge in the form of springs and seeps due to the structural barriers and permeability contrasts they create (Forster and Evans, 1991; Bense et al., 2013).

Due to the lack of detailed regional geologic maps, pluton-scale and simplified (i.e., geologic lumped by petrologic composition) geologic maps were created for the study area (Fig. 3). These maps were created by digitizing geologic quadrangles from Moore (1963), Bateman and Moore (1965), Bateman et al. (1965), Ross (1965), Nelson (1966), Lockwood and Lydon (1975), Moore (1981), and Stone et al. (2000) (Fig. 3). The following geologic descriptions are summarized from the synthesis of these geologic maps. The geology of the eastern Sierra Nevada is predominantly composed of Cretaceous plutonic rocks ranging from felsic alaskite to more mafic diorite, quartz diorite and hornblende gabbro (Fig. 3). Most plutons are in the granitic petrologic range from quartz monzonite to granodiorite. In addition to Cretaceous plutonic rocks, areas of the eastern Sierra enclose pre-Cretaceous rocks of two different varieties: Paleozoic metasedimentary roof pendants and metavolcanic rocks of Mesozoic age. The rock types (and permeability) of the roof pendants vary significantly and include facies of marble, calc hornfels, pelitic hornfels, micaceous quartzite, and biotite schist (Moore, 1963; Bateman et al., 1965). On the eastern side of the valley, the White and Inyo Mountains are primarily composed of Paleozoic carbonates.

There are a number of geologic units that are only found locally, yet are easily weathered (e.g., glacial deposits and mafic rocks) and thus have the potential to significantly influence groundwater geochemistry, where present. For example, extensive glacial till deposits are found at high and mid elevations of the eastern Sierra Nevada, most notably the Tioga Till and the Tahoe Till. In the northern part of Owens Valley, the Bishop Tuff, a pyroclastic flow and ash-fall deposit related to the eruption of the Long Valley Caldera, outcrops over a large area with a thickness up to 200 m. Lava flows and cinder cones are also present in the valley, most notably at the Big Pine Volcanic Field, a zone of alkali-olivine basalts associated with Cenozoic extension (Ormerod et al., 1991).

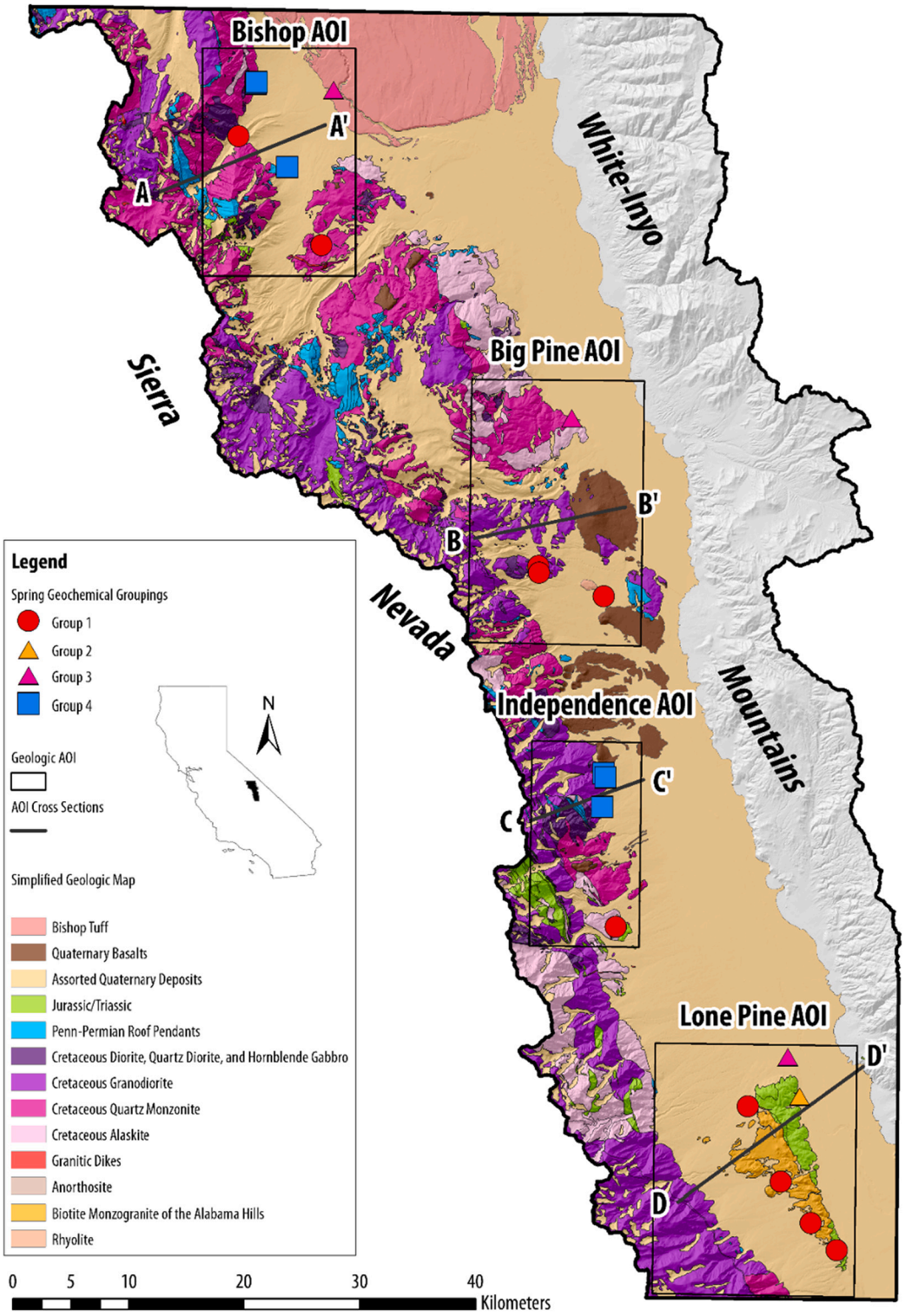

Fig. 3. Simplified geologic map of Owens Valley with major petrologic compositions and significant geologic units (e.g., the Bishop Tuff) grouped by colour. This geologic map was created by simplifying units across 10 geologic quadrangles. For granitic plutons, colour ranges from light pink (alaskite) to dark purple (mafic rocks like diorite, quartz diorite, and hornblende gabbro). This colour scheme is adapted from Bateman et al. (1965). Spring locations are symbolized by their spring geochemical groupings. Four geologic areas of interest (AOIs) are shown in the black rectangles. Cross section lines are shown in the black lines across each geologic AOI. These lines correspond to cross sections in Fig. 9. (For interpretation of the references to colour in this figure legend, the reader is referred to the web version of this article.)

The southeastern Sierra Nevada are geologically complex. To aid the reader we included detailed geologic descriptions for four geographic areas of interest (AOIs) where sampled springs and host aquifers are located (see Appendix A). Each AOI is outlined in Fig. 4, shown with increased detail in Fig. 8, and has an associated geologic cross section (Fig. 9). Table 1 provides petrologic information for likely flowpath units that are described for each AOI.

3. Methods

3.1. Utilizing data from Feth et al. (1964)

Water temperature and major ion data of ephemeral and perennial mountain spring samples from Feth et al. (1964) are compared with mountain-front spring samples from this study to understand how increasing groundwater flowpath length and circulation (inferred by spring water temperature) influence spring water geochemical composition from local to intermediate spatial scales. Ephemeral (1 out of 15) and perennial spring (24 out of 64) samples from Feth et al. (1964) are excluded if they emerge below 1830 mamsl (6000 ft). This elevation threshold is indicative of the mountain block-alluvial fan transition zone in Owens Valley and is near the upper limit of the elevation range (1130–1990 mamsl) of the springs from this study.

3.2. Field sampling procedures

Water samples from 20 springs emerging on the west side of Owens Valley were collected during the spring of 2016. Springs on Los Angeles Department of Water and Power land were sampled in March while the remainder of the springs, located inside the Inyo National Forest (INF) boundary, were sampled during May. The majority of the sampled springs are classified as rheocrenes (Springer and Stevens, 2009). However, among all springs there is diversity in the emergence style (i.e., subaerial, subaqueous, or seepy/diffuse). The quality of the emergence has implications for tracer sample collection, especially with gaseous tracers. In all cases, springs were sampled as close to the spring emergence as possible. A Masterflex platinum-cured silicone tubing was placed at the spring source and sometimes positioned with a rock or zip tie if the discharge was too turbulent or fast. Samples were collected using a GeoTech peristaltic pump and filtered, depending on the tracer, using 0.22 μm polyethersulfone membrane Sterivex-GP pressure filter units.

Parameters measured in the field yield information about groundwater conditions at the time of emergence. Field geochemical data were measured with a YSI Professional Plus multi-parameter probe including temperature (°C), pressure (mm/Hg), pH, conductivity (μS/cm), and dissolved oxygen (mg/L and % of saturation). Specific conductance @ 25 °C (μS/cm) and total dissolved solids (mg/L) are automatically calculated from the conductivity measurement by the YSI. All equipment, including tubing, probe, and shoes were sanitized with quaternary ammonia and ethanol to prevent transmission of invasive species into and between spring sampling sites.

3.3. Stable isotopes of water (δ^2H and $\delta^{18}O$)

Stable isotopes of oxygen of hydrogen were collected unfiltered in 2 mL vials with no head space and kept on ice or refrigerated until shipped for analysis. Spring water analysis of δ^2H and $\delta^{18}O$ was performed at the University of California, Davis Stable Isotope Facility (SIF). using a Laser Water Isotope Analyzer V2. The reported uncertainty for this analysis is 0.83‰ for δ^2H and 0.08‰ for $\delta^{18}O$.

To aid in the regional interpretation of water stable isotopes, groundwater δ^2H and $\delta^{18}O$ data from a geographic bounding box surrounding Owens Valley were extracted from the USGS Water Quality Portal These data were used to create a Local Ground Water Line (LGWL) to examine regional patterns in groundwater stable isotope composition (i.e., (Blasch and Bryson, 2007; Liu and Yamanaka, 2012; Gleason et al., 2020). In addition, data from Bowen and Revenaugh (2003) and Bowen et al. (2005) were used to construct a winter $\delta^{18}O$ isoscape of the study area.

3.4. General chemistry

General chemistry samples were field filtered and collected in 250 mL high-density polyethylene (HDPE) bottles and refrigerated upon sampling until sent for analysis. Major cations and anions were measured at the New Mexico Bureau of Geology and Mineral Resources Chemistry Lab. Cations were measured using inductively coupled plasma optical emission spectrometric techniques (ICP-ES) according to EPA 200.7. Anions were measured using an ion chromatograph (IC) according to EPA 300.0. Duplicates were run on every 10th sample. Low bromide analysis was performed for water samples under the bromide detection limit of 0.1 mg/L. Charge balance errors (CBE) for all springs were under 5%.

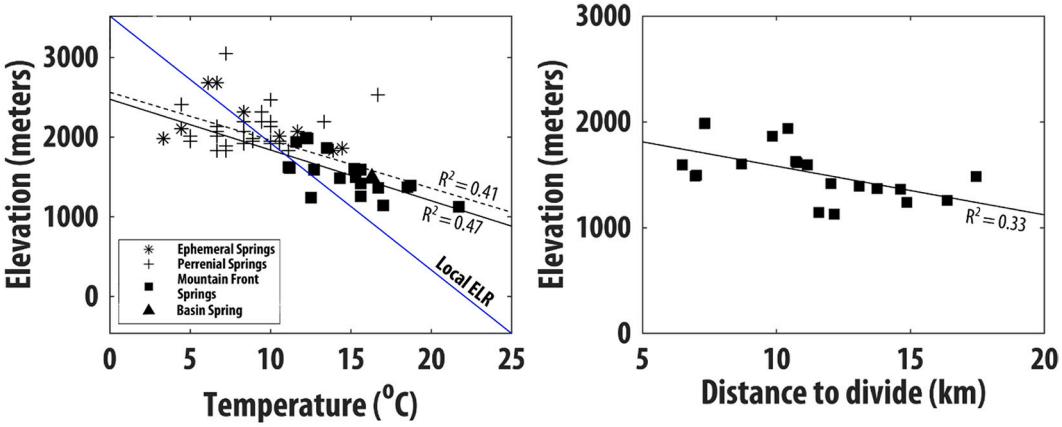

Fig. 4. A) Spring discharge temperature versus spring elevation. Mountain front springs from this study are symbolized by the black squares and the basin spring is symbolized by the black triangle. Ephemeral and perennial springs samples from Feth et al. (1964) are shown by the asterisk "*" and plus "+" symbols, respectively. The local environmental lapse rate (ELR) based on average annual temperature is shown as the blue reference line. The solid black line represents the linear relationship for just the mountain front springs ($R^2 = 0.47$) and the dashed black line represents the linear relationship when including all samples on the plot ($R^2 = 0.41$). B) Spring elevation is plotted against distance to the eastern regional divide, the crest of the Sierra Nevada. (For interpretation of the references to colour in this figure legend, the reader is referred to the web version of this article.)

Table 1
Petrologic and mineral data (%) for Owens Valley plutons.

Geologic Unit	Petrologic Source	Unit Abbreviation	Quartz	K-Feldspar	Plagio-clase	Biotite	Horn-blende	Pyro-xene	Accessory and Secondary Minerals	Mafic Minerals	Plag (An)	Springs Influenced (IES#)
Whitney Granodiorite	Moore, 1987	Kw	24.9	23.5	44.9	–	–	–	–	6.7	25–27*	21,22,23,24,25,26
Paradise Granodiorite	Moore, 1987	Kp	23	20.9	46.2	–	–	–	–	9.9	29–31*	21,22,23,24,25,26
Granodiorite of Sugarloaf	Moore, 1987	Ksl	21.6	20	44.6	–	–	–		13.9	36*	21,22,23,24,25,26
Lone Pine Creek Granodiorite	Moore, 1987	Klp	21.6	10.7	47	–	–	–	–	20.7	N/A	21,22,23,24,25,26
Dikes and Sills	Moore, 1987	Kgd	38.1	29.8	30.7	–	–	–	–	1.4	16–26*	27
Dragon Pluton	Moore, 1987	Kd	8.3	28	54.6	–	–	–	–	9	19*	26?,27
Dragon Pluton	Moore, 1963	Kd	12.7	24.5	51.5	7.3	1.9	Tr	2	–	23	26?,27
Independence Pluton	Moore, 1987	Ki	28.9	35.6	32.8	–	–	–	–	2.7	16*	28,42,43
Independence Pluton	Moore, 1963	Ki	30	42.7	24.7	1.8	–	–	0.9	–	14	27,28,42,43
Tinemaha Granodiorite (Woods Lake Mass)	Moore, 1963	Ktnwl	23.6	21.8	41.8	8.2	2.8	–	1.9	–	30	27
Alabama Hills Granite (Kah)	Abbott, 1972	Kah	–	–	–	–	–	–	–	–	–	21,22,23,24,25,26
Spook Pluton (Outer)	Moore, 1963	Ksp	24.5	18.3	46.7	6.9	2.4	–	1.3	–	32	28,42,43
Spook Pluton (Inner)	Moore, 1963	Ksp	24.4	20.4	49.2	4.7	0.1	–	1.2	–	26	28,42,43
Bullfrog Pluton	Moore, 1987	Kb	24.9	39.6	33	–	–	–	–	2.5	14*	24,25,26,27
Bullfrog Pluton	Moore, 1963	Kb	25	37.3	34.7	1.8	0.2	–	1	–	10	24,25,26,28
Rocks Similar to Cathedral Peak Granite (Alaskite)	Bateman et al., 1965	Kca	33	38.6	25.8	1.8	0.2	–	2.2	2.9	~15	37,38,30
Tungsten Hills quartz monzonite (Pine Creek)	Bateman et al., 1965	Kt	31.9	29.1	32.5	4.8	3.9	–	1.4	6.5	28–30	30,33
Tungsten Hills quartz monzonite (Bishop Creek)	Bateman et al., 1965	Kt	29.8	31	33.2	5.5	0.2	–	2.1	6.2	28–31	32
Tungsten Hills quartz monzonite (Shannon Canyon)	Bateman et al., 1965	Kt	27.7	33.5	32.9	4	0.1	–	2.9	5.9	~15	30
Round Valley Peak granodiorite	Bateman et al., 1965	Krv	26.8	18.7	44.4	7.2	3.6	–	1.9	10.1	33–38	37,38
Wheeler Crest Quartz Monzonite (kwc)	Bateman et al., 1965	Kwc	29.3	25.3	35.3	5.8	1.6	–	1.6	10.1	28–36	37,38,33,39
Granodiorite of McMurray Meadows	Bateman et al., 1965	Kmm	20.5	26.4	40.1	8	3.1	–	1.6	12.7	37	40,41
Tinemaha Granodiorite	Bateman et al., 1965	Ktn	21.3	23.6	39	4.6	6	–	3.4	16.1	38	40,41,29
Mafic plutonic masses	Moore, 1963	Km	8	8.625	54.975	11.2	8.5	5.75			30–70	28,42,43
Diorite, quarz diorite, hornblende gabbro	–	Kd	–	–	–	–	–	–	–	–		37,38,33,39,40,41
Felsic Dikes	–	ap										32,40,41

3.5. $^{87}Sr/^{86}Sr$ analyses and rock leaching of $^{87}Sr/^{86}Sr$

Samples for strontium isotope analysis of spring waters were field filtered and collected in 125 mL HDPE bottles. Strontium isotopes were prepped and analyzed in the Mulicollector ICPMS Laboratory at the University of Illinois Urbana-Champaign (UIUC). Strontium was eluted from each sample before a concentration check was performed using inductively coupled plasma mass spectrometry (ICPMS) to achieve a goal concentration of 100 ppb. Samples with concentrations greater than 100 ppb were diluted to achieve a 100 ppb concentration while samples with low concentrations (i.e., lower voltages) were designated to have longer analytical runs A Nu Plasma HR multicollector inductively-coupled-plasma mass-spectrometer (MC-ICPMS) was used for strontium isotope analysis. Reported analytical uncertainty for $^{87}Sr/^{86}Sr$ ratios is 10^{-5}.

In situ rock samples were collected from different geologic units in the study area for strontium leaching experiments (e.g., Frisbee et al., 2017). Whole rock samples were leached using deionized water to supplement existing whole-rock literature values. Samples were collected from plutonic rocks and metasedimentary roof pendants that represent likely flowthrough aquifers supplying groundwater to sampled springs. Rock preparation and leaching was conducted at Purdue University. Rock samples were crushed and sieved. For each geologic unit, 200 mg of crushed rock was added to 1 L HDPE bottles filled with deionized water. The bottles were capped tightly, sealed with electrical tape, and stored for two months in the laboratory. After the allotted time, leachate samples were decanted and filtered. Chemical preparation and MC-ICPMS analysis was performed at UIUC in the same manner as the spring water samples.

3.6. Dissolved noble gas collection and modeling

Noble gas samples were collected in copper tubes only at springs with clear emergences lacking turbulent flow and excessive bubbles. Samples were analyzed for Ar, Kr, Xe, Ne, ^{4}He, $^{3}He/^{4}He$ ratio at the University of Utah Noble Gas Lab. The measurement error for helium is ±1% of the reported value. For all other gases the measurement error is between 1% and 5% of the reported value. $^{3}He/^{4}He$ ratios (R) are reported normalized to the atmospheric $^{3}He/^{4}He$ ratio (R_a) ($1.38 * 10^{-6}$) as R/R_a.

Raw noble gas measurements were interpreted with Noble90, a non-linear, error-weighted least squares inversion MATLAB program for interpretating noble gas concentrations by solving for recharge temperature, recharge pressure (elevation), recharge salinity, excess air, and fractionation (Aeschbach-Hertig et al., 1999; Aeschbach-Hertig et al., 2000; Kipfer et al., 2002; Peeters et al., 2003). Noble90 allows for a variety of fitting options. In this study we used the ta-1 fit (closed equilibration model) with 100 Monte Carlo simulations per sample. A ta-2 fit (partial reequilibration model) was used if the ta-1 fit yielded nonrealistic results. We utilized four solving parameters: Ne, Ar, Kr, and Xe. Helium (He) was not used as a solving parameter due to geogenic and terrigenic sources of helium within the study area. Recharge salinity was assumed to be zero for Owens Valley spring waters. Because recharge pressure (elevation) is unknown, two approaches were taken. The first approach was to solve for recharge temperature across a suite of elevations from the spring emergence to the regional peak. The intersection of this family of solutions with the local environmental lapse rate (ELR) provides an approximate recharge elevation (Zuber et al., 1995; Manning and Solomon, 2003; Doyle et al., 2015; Peters et al., 2018). Due to the lack of weather stations across a large elevation gradient, a synthetic lapse rate was constructed by extracting values of elevation and mean annual temperature (O'Donnell and Ignizio, 2012) from randomly distributed points (~6000) within a bounding region of the study area. A linear regression was fit to these points to derive a local annual ELR. Due to the potential uncertainty of the synthetic lapse rate and the large elevation gradient of the study area, calculated recharge elevations derived from this method are only utilized to approximately constrain the recharge elevation zone and recharge type (e.g., cold, snowmelt recharge) supporting perennial springflow. An alternate approach for solving for the other recharge parameters is the use the median elevation of the watershed or contributing area (Thomas et al., 2003; Paukert, 2014) or to assume a recharge elevation based on topography (Singleton and Moran, 2010; Manning et al., 2012). For this approach we used an elevation of 2600 m, the approximate median elevation between the Owens Valley basin floor and the Sierra Nevada crest east of Owens Valley. While both approaches were both used for calculating recharge temperatures, only the median elevation method was used for deriving excess helium concentrations.

3.7. Geochemical modeling

Inverse modeling of general chemistry data is commonly employed to reconstruct the chemical composition of water into a series of weatherable minerals and precipitable clays that have reacted or formed to create the resulting chemistry. Many of the springs in this study emerge at fault zones along the eastern Sierra Nevada mountain front, and there are no previously sampled springs or wells upgradient that are plausible candidates for a starting water for tracking weathering. Therefore, precipitation was used as the pre-weathering chemical composition of spring waters, and the geochemical composition of springs was modeled using the known mineralogy of geologic units in the study area as model constraints. While there is precipitation chemistry data available through the National Atmospheric Deposition Program (NADP) for one station inside HUC 180901, NTN Site CA34 (Bishop, CA), these data are problematic for several reasons: 1) data are only available for a small period between 1980 and 1982, 2) the standard deviation in many of the reported analytes over that three year period is very high (in some cases the Cl^- and SO_4^{2-} values in precipitation are higher than spring water values), 3) Bishop, CA lies in the basin of Owens Valley and thus doesn't provide a good endmember for high elevation recharge, and 4) Bishop precipitation chemistry data might be influenced by aeolian deposition from Owens (Dry) Lake. Rather than use data from CA34, NADP data were averaged from three high elevation sites in the southern Sierra Nevada: CA99 (Yosemite National Park- Hogdon Meadow, elev. 1393 mamsl), CA28 (Kings River Experimental Watershed, elev. 2000 mamsl), and CA75 (Sequoia National Park- Giant Forest, elev. 1921 mamsl) to calculate an initial precipitation endmember as a model starting point. Alkalinity and bicarbonate are not reported for NADP data; however, bicarbonate was added to averaged precipitation chemistry to rectify the charge imbalance. Chloride is considered a conservative ion and is often used for calculating geochemical enrichment in the subsurface as subsurface increases in chloride can be attributed to the effects of evaporation and transpiration. Many study springs had chloride values close to or below the detection limit (0.1 mg/L), therefore, we consider the effects of evapotranspiration negligible and attributed all chloride enrichment to flowpath mixing and wind deflation due to the proximity of the study area to multiple playas and Owens (Dry) Lake.

Netpath-XL (Parkhurst and Charlton, 2008), a derivative of NETPATH (Plummer et al., 1994), was used to identify reasonable and mass-balanced inverse geochemical models describing the amount and suite of weathered minerals necessary to form an observed final water composition from an initial starting water. In Netpath-XL, the user specifies both elemental constraints and mineral phases to calculate possible geochemical models, which requires a detailed assessment of the aquifer mineralogy, including the stoichiometry of these minerals. For example, small differences in plagioclase composition, such as choosing An_{30} versus An_{40}, can substantially alter model results and the number of possible solutions. While Netpath-XL has its own mineral database, it is sometimes necessary to add in minerals or alter existing mineral stoichiometry to effectively model the likely aquifer dissolution reactions based on known mineralogy.

Netpath-XL models can often yield multiple solutions. Calculated saturation indices and stability diagrams were used to help inform and critique model results. For this study, stability diagrams were created using Geochemist Workbench Student Edition 11.0 (GWB) and saturation indices for a suite of mineral phases were calculated with PHREEQC. Certain phases likely to be present based on known mineralogy were forced into the model solution. Similarly, certain phases were restricted to only dissolve or only precipitate to limit model solutions.

The main phases used for Netpath-XL to model the chemical compositions of Owens Valley spring waters include CO_2 gas, quartz (SiO_2), gypsum, halite, calcite, plagioclase (An_{15}-An_{45} depending on the candidate aquifers), potassium feldspar, biotite (phlogopite), hornblende, augite, kaolinite, and Ca-montmorillonite. Published geologic quadrangles (e.g., Moore, 1963; Bateman et al., 1965; Stone et al., 2000) and associated cross sections helped constrain the likely aquifer units supporting flowpaths to springs, which were assumed based on the regional topographic gradient and informed by stable isotope and noble gas results. Petrologic data, such as modal analyses of minerals from thin sections and CIPW norms, helped to inform model phases and forcing constraints. CIPW norms were only used to inform plagioclase stoichiometry when thin section modal analysis data were not available. Mineralogic data were compiled from multiple studies (Moore, 1963; Bateman et al., 1965; Michael, 1983; Moore, 1987; and Hirt, 2007) and are summarized in Table 1. Additional units influencing flow without petrologic data are summarized in Table 2.

4. Results

4.1. Field observations

Of the 20 study springs, twelve emerge directly along the mountain front near the Sierra Nevada Frontal Fault Zone (1258–1989 mamsl). Four springs (IES-021, IES-022, IES-023, and IES-024) emerge at smaller faults on the west side of the Alabama Hills at a slightly lower basin elevation range (1240–1393 mamsl). IES-029 emerges at a large high-angle fault near the Big Pine Volcanic Field at an elevation of 1418 mamsl. Two springs (IES-025 and IES-026) emerge near the basin center (1128–1145 mamsl), however, only IES-025 shows signs of significant basinal rock-water interaction and is considered a "basin" spring. One spring (IES-034) emerges directly out of the Bishop Tuff at the northern end of the valley (1482 mamsl) (Fig. 3). Spring elevation is moderately correlated ($R^2 = 0.33$, $p < 0.05$) with distance from the regional divide (Fig. 4B). For the purposes of this geochemical study, springs slightly further away from drainage divide (i.e., the Alabama Hills springs, IES-026, IES-029, and IES-034) are still considered "mountain front" springs. Although these springs may be discharging some proportion of water recharged through basin fill: (1) such stream infiltration water is relatively dilute, (2) the basin fill material is directly sourced from the adjacent mountain block, and (3) many of these springs emerge from depth along major fault zones (e.g., the Sierra Nevada Frontal Fault Zone).

Table 2
Potential geologic units affecting spring chemistry.

Units	Springs Influenced (IES#)
Qyb (young basalts)	29
Bishop Tuff	34
ch (Calc-hornfels)	28,33,42,43
phq (Pelitic hornfels)	29,32
Pm,m (marble)	37,38,33,28,42,43
PPmq (micaceous quartzite)	37,38
Pzbs (biotite schist)	28,42,43
JTrt (metarhyolite)	27
Volcanic Complex of the Alabama Hills (upper part)	21,25,26
Volcanic Complex of the Alabama His (lower part)	21,25,26

All mountain-front springs ($n = 19$) and basin ($n = 1$) from this study are low temperature springs with discharge temperatures ranging from 11.1 to 21.7 °C (mean discharge temperature = 14.9 °C). The temperature range from this study is elevated compared to the temperature ranges of ephemeral springs (3.3 °C–14.4 °C; average of 8.8 °C) and perennial springs (4.4 °C–16.7 °C; average of 8.8 °C) reported by Feth et al. (1964). There is a negative correlation ($R^2 = 0.46$, $p < 0.05$) between spring water temperature and elevation (Fig. 4A) among mountain front springs. This linear relationship persists between spring head elevation and temperature ($R^2 = 0.41$, $p < 0.05$; $n = 43$) when the mountain front springs are plotted with the ephemeral and perennial springs from Feth et al. (1964). The majority of the mountain-front springs (17/19) fall above the local annual ELR, whereas a smaller fraction of the ephemeral and perennial mountain block springs (27/43) fall above the local ELR. All mountain front spring waters are neutral to slightly alkaline with pH values falling in the range of 6.8–8.0. Field data is summarized in Table 3.

4.2. General chemistry trends

Geochemically, Owens Valley mountain front springs are either Ca-HCO_3 ($n = 15$) or Na-HCO_3 ($n = 4$) type waters. One basin spring, IES-025, is classified as an Na—Cl type water. The mountain-front springs are relatively dilute and have TDS concentrations <250 mg/L. IES-025 has a TDS concentration of 724 mg/L. Moderate to strong positive linear trends ($R^2 > 0.55$; $p < 0.05$) exist between all major ions and specific conductance with the exception of sulfate and silica (Fig. 5 inset plots). Calcium and bicarbonate are the strongest predictors of specific conductance ($R^2 = 0.73$ and $R^2 = 0.88$, respectively) for the mountain-front springs. The relationships between major ions and specific conductance are best described by power-law trends when the ephemeral and perennial springs from Feth et al. (1964) are included in the analysis (Fig. 5). Power-law trends with sodium, potassium, chloride, and sulfate are significant ($p < 0.05$) and are stronger when the basin spring (IES-025) is included in the analysis (R^2 values of 0.84, 0.66, 0.81, and 0.84, respectively). Power-law trends with calcium, magnesium, and bicarbonate are significant ($p < 0.05$) and improved by excluding the basin spring sample from analysis (R^2 values of 0.88, 0.60, and 0.92, respectively). General chemistry data is shown in Table 4.

Mineral saturation indices were calculated for Owens Valley mountain front spring waters in PHREEQC using the default thermodynamic database. All spring waters are undersaturated with respect to anhydrite, calcite, gypsum, halite, and sepiolite while saturated with respect to quartz. Only the most dilute samples are undersaturated with respect to chalcedony. IES-025, the basin spring sample, is saturated with respect to aragonite and dolomite.

Stability diagrams of the kaolinite and montmorillonite stability fields at 25 °C were constructed to identify the most kinetically favorable clays likely to precipitate out of solution. Garrels and Mackenzie (1967) considered kaolinite the primary weathering product when modeling the evolution from precipitation to ephemeral springs based on aluminosilicate residue compositions. They also considered the evolution of ephemeral springs to perennial springs to yield weathering products of kaolinite and Ca-montmorillonite. The majority of Owens Valley mountain-front spring waters lie in the kaolinite stability field rather than in the Ca-montmorillonite (shown as beideillite-Ca) stability field (Fig. B.1). The exceptions are springs with lower Ca^{2+}/Na^{+} molar ratios.

4.3. Stable isotope observations

Owens Valley spring waters have a δ^2H range from −134.2 to −116.8‰ ($n = 20$). Spring water $\delta^{18}O$ values range from −18.0 to −15.2‰. A line was fitted to the IES spring data to create a Local Spring Water Line (LSWL; $\delta^2H = 6.38 * \delta^{18}O - 17.39$). This line is nearly parallel to, yet offset from, the Local Meteoric Water Line (LMWL) defined by

Table 3
Field geochemical data.

Sample ID	Spring Name	Date	UTM 11 S E	UTM 11 S N	Elevation (m)	Temp. °C	Specific Conductance (mS/cm)	pH	TDS (ppm)	ORP (mV)	DO (%)	DO (mg/L)	AOI
IES-021	Lubkin Canyon Spring 1	3/19/2016	405,405	4,044,353	1241	12.5	479	7.85	311	124.3	56.1	5.98	Lone Pine
IES-022	Indian Spring	3/19/2016	403,165	4,046,717	1362	16.7	191.8	7.36	125	143.7	52.1	5.07	Lone Pine
IES-023	Lone Pine Ck. Complex	3/19/2016	400,577	4,050,223	1371	18.5	239.7	7.42	156	112.5	65.1	6.08	Lone Pine
IES-024	Spring along Hogback Ck. A	3/19/2016	397,732	4,056,750	1393	18.7	397.4	6.95	260	174.2	72.9	6.79	Lone Pine
IES-025	Boron Springs B	3/19/2016	402,195	4,057,591	1128	21.7	2670	7.81	1729	185.1	64.9	5.65	Lone Pine
IES-026	Reinhackle Spring	3/19/2016	401,193	4,061,012	1145	17	515.1	7.75	334.	195.5	69.8	6.73	Lone Pine
IES-027	Boron Springs A	3/20/2016	386,328	4,072,314	1602	15.2	470.7	7.88	318	186.6	63	6.31	Independence
IES-028	Grover Anton Spring	3/20/2016	385,165	4,082,719	1594	15.6	480	7.63	312	235.6	72.3	7.21	Independence
IES-029	Unnamed spring north of Red Mountain	3/20/2016	385,305	4,100,901	1418	15.6	273.5	7.75	154	206.4	58.8	5.84	Big Pine
IES-030	Unnamed spring north of Big Pine	3/20/2016	382,448	4,116,323	1259	15.6	428.2	7.68	280	204.8	79.2	7.85	Big Pine
IES-032	Sharps Meadow	3/21/2016	360,840	4,131,349	1939	11.6	179.9	8.14	117	183.7	72.8	7.92	Bishop
IES-033	Elderberry Canyon Spring	3/21/2016	357,900	4,138,046	1596	12.7	164.8	7.73	107	249.7	81.8	8.65	Bishop
IES-034	Birchim Cyn. Spring B	3/21/2016	364,114	4,144,865	1483	16.3	427	7.53	277	201.6	70	6.59	Bishop
IES-037	Wells Meadow A	5/17/2016	355,178	4,145,270	1625	11.1	67.3	7.11	44	99.1	67.6	7.37	Bishop
IES-038	Wells Meadow B	5/17/2016	355,222	4,145,412	1615	11.2	66.1	7.87	43	52.5	69.6	7.59	Bishop
IES-039	Unnamed spring along Pine Ck.	5/17/2016	353,679	4,140,727	1864	13.5	83.2	7.17	54	47.7	33.8	3.45	Bishop
IES-040	McMurray Mdw.Spring A	5/17/2016	379,576	4,103,521	1989	12.2	216.2	7.5	140	107.2	58.3	6.25	Big Pine
IES-041	North Fuller Mdw. Spring	5/17/2016	379,636	4,102,941	1982	12.3	292.4	6.63	190	112.7	25.4	2.7	Big Pine
IES-042	North Harry Birch Spring	5/18/2016	385,273	4,085,645	1487	14.3	191.9	7.61	125	−2.1	53	5.43	Independence
IES-043	South Harry Birch Spring	5/18/2016	385,440	4,085,284	1498	15.3	243.5	6.94	159	77.7	29.5	2.94	Independence

Friedman et al. (2002) ($\delta^2H = 7.12 * \delta^{18}O - 3.6$) for the Great Basin. A Local Groundwater Water Line (LGWL) ($\delta^2H = 7.326 * \delta^{18}O - 2.7$) was created from USGS well and spring data extracted from within the Owens Valley drainage basin (https://waterdata.usgs.gov/nwis/qw). Both the LSWL and the LGWL have lower slopes than the Global Meteoric Water Line (GMWL) from Craig (1961) (Fig. 6A). Calculated deuterium excess values ($\delta^2H - 8*\delta^{18}O$) span from 13.0 to 4.7‰, though the majority of samples (14/20) have values between 9.0 and 12.0‰, indicative of a similar vapor source region among samples. Springs further away from the mountain front emerging near the basin center have deuterium excess values ranging from 4.7 to 7.1‰. Stable isotope data is summarized in Table 5.

IES and USGS δ^2H and $\delta^{18}O$ values for Owens Valley groundwaters cluster spatially by geographic region (Fig. 6B). Samples in the Bishop geographic region, furthest north, are the most isotopically depleted. Samples in the Lone Pine region, furthest south, are the most isotopically enriched. While there is a moderate correlation ($R^2 = 0.31$; Fig. 6B inset plot) between the elevation and $\delta^{18}O$ composition of mountain front and basin spring samples, this is likely a reflection of the influence of geography. There are no discernable trends with elevation and spring isotopic composition when examining individual geographic regions, precluding the use of stable isotopes as a means to constrain recharge elevation (e.g.,James et al., 2000).

4.4. Dissolved noble gases in spring waters

4.4.1. Calculated recharge parameters from Noble90

The methodology behind deriving noble gas recharge elevations from the ELR method (e.g., Zuber et al., 1995; Manning and Solomon, 2003; Doyle et al., 2015; Peters et al., 2018) is displayed for an example spring, IES-029, in Fig. 7. Mountain front spring recharge elevations range from 1900 to 3400 mamsl with an average recharge elevation of 2820 mamsl (Table 6; Fig. B.2). Springs further away from the mountain front (i.e., springs near the Alabama Hills) have lower calculated recharge elevations which suggests that a lesser fraction of spring discharge may be from recharge through the basin fill. Recharge temperatures using the median elevation between the Owens Valley basin floor and the Sierra Nevada crest (2600 m) as a solving parameter range from 1.6 °C to 7.7 °C, with an average recharge temperature of 4.3 °C. Recharge temperatures derived using the ELR method have an average of 4.0 °C and are all within a range of ±3.5 °C of the recharge temperatures calculated using the median elevation (Table 6). The amount of offset between the temperature calculations depends on whether the calculated recharge elevation using the ELR method is above the median elevation (cooler) or below the median elevation (warmer). Noble gas recharge parameters are shown in Table 6.

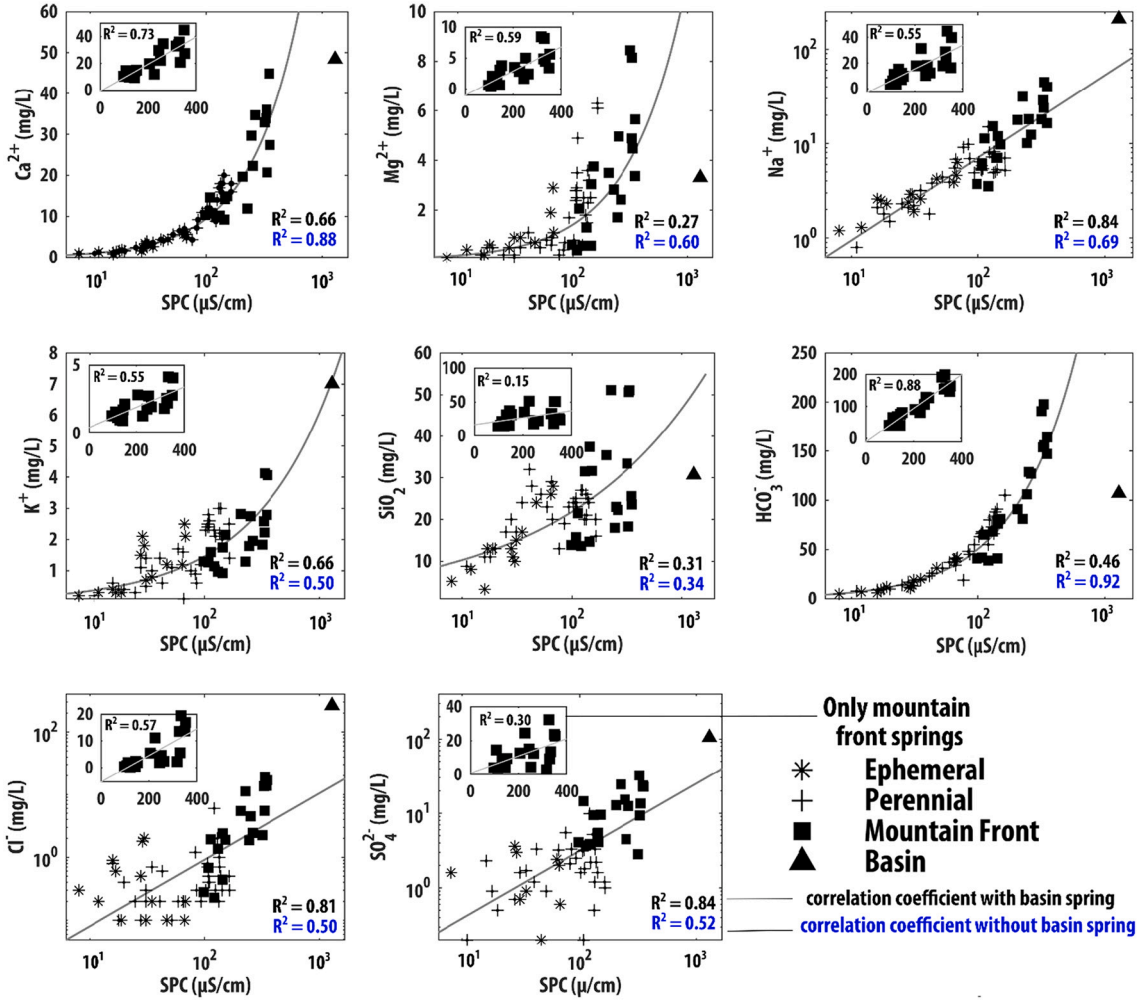

Fig. 5. The main plots show power-law trends between specific conductance and solute concentrations when including ephemeral and perennial springs from Feth et al. (1964) in the analysis. Correlation coefficients (R^2 values) are provided on the main plots for all springs in black (i.e., including the basin spring) and excluding the basin spring in blue. Inset plots show the linear relationships between specific conductance and solute concentrations for major cations and anions for Owens Valley spring waters. (For interpretation of the references to colour in this figure legend, the reader is referred to the web version of this article.)

4.5. Geochemical groupings for mountain front springs

Owens Valley mountain front spring waters are classified into four geochemical groups based on likely flowpath rock-water interaction inferred from stable isotope results, noble gas recharge parameters, and geologic maps (Fig. 8) and associated cross sections (Fig. 9), the Piper diagram (10), and solute weathering plots (Fig. 11). These geochemical groupings are independent of the geographic AOIs and reflect geochemical evolution via the mineralogy of the inferred spring contributing areas.

Group 1 consists of springs with a granitic (alaskite-quartz monzonite-granodiorite) weathering signature typical of interaction with Sierra Nevada plutonic rocks. This group is the largest ($n = 10$) and exhibits the greatest intragroup variation in weathering trends (Fig. 10). Group 2 consists of one spring, IES-025, a basinal brine emerging on the eastern side of the Alabama Hills with high a TDS concentration (724 mg/L). Group 3 comprises three springs (IES-026, IES-030, and IES-034) that are Na-HCO_3 type waters with elevated sodium, potassium, and silica concentrations. The geochemical compositions of these springs are interpreted to be influenced by volcanic weathering from ash flows or tuffs, felsic dikes and masses, or contributions from surface water features (e.g., the LAA or the Owens River). Birchim Cyn. Spring B (IES-034) and Reinhackle Spring (IES-026) are both located near the Owens River or LAA and have enriched δ^2H and $\delta^{18}O$ values compared to other spring waters. Our interpretation is consistent with past studies that also attribute some portion of flow at Reinhackle Spring to aqueduct leakage (Bassett et al., 2008). Springs in Group 4 have Paleozoic metasedimentary roof pendants enclosed within granitic rocks in their likely recharge areas (Fig. 8). These springs have chemical signatures (i.e., significantly excess calcium) reflecting a mixture of carbonate (e.g., marble, micaceous quartzite, calc-hornfels) and granitoid dissolution.

The geochemical differences among these four groups can be seen on Fig. 10 and in the geochemical plots (Fig. 11). While trends showing geochemical evolution exist between major ions like Ca^{2+} vs Mg^{2+} and Ca^{2+} vs $HCO3^-$ when considering all springs, these evolution pathways are stronger after springs are broken out into their respective geochemical groupings, as shown in Fig. 11A and B. Fig. 11C shows intergroup separation when magnesium/potassium molar ratios are plotted against calcium/sodium molar ratios. A reference line for the Mg^{2+}/K^+ ratio expected from biotite weathering (~3) is plotted horizontally in addition to a vertical bounding area of expected Ca^{2+}/Na^+ ratios for Owens Valley granitoids based on an average range of plagioclase compositions from An_{28} to An_{36} (Table 1). The majority of springs ($n = 17$) have Mg^{2+}/K^+ ratios at or below the reference line and likely do not receive significant amounts of magnesium from pyroxenes or amphiboles like hornblende. IES-024 and IES-041 plot well above the reference line for Mg^{2+}/K^+ molar ratios and have sources of hornblende in their likely recharge area. Ca^{2+}/Na^+ molar ratios for spring waters in

Table 4
General chemistry data.

Sample ID	Ca^{2+}	Mg^{2+}	Na^{+}	K^{+}	Sr^{2+}	Br^{-}	Cl^{-}	Cl^{-}/Br^{-}	F^{-}	SO_4^{2-}	HCO_3^{-}	Si as SiO_2	TDS	Charge Balance	pH	Lithium	Boron	Geo-chemical
	(mg/L)	(mg/L)	(mg/L)	(mg/L)	(mg/L)	(mg/L)	(mg/L)		(mg/L)	(mg/L)	(mg/L)	(mg/L)	(mg/L)	(%)		(ppb)	(ppb)	Group #
IES-021	19.7	3.5	17.9	2.82	0.284	0.021	5.48	261	0.13	12.8	91	35.4	143	4.9	6.8	10	101	1
IES-022	10.2	1.31	15.3	0.975	0.119	–	1.36	181*	0.45	9.45	68	31.5	105	−2.28	6.9	14	92	1
IES-023	14.2	3.04	12	1.74	0.162	0.022	2.4	109	–	4.15	76	37.4	113	4.38	6.8	7	36	1
IES-024	36	8.15	24	2.22	0.411	0.044	5.52	125	–	9.33	198	50.6	238	−1.06	7.1	50	101	1
IES-025	48.4	3.31	209	7.01	1.59	0.18	264	1467	3.16	105	107	30.7	724	1.72	7.2	441	3584	2
IES-026	27.4	5.65	39.7	4.07	0.195	0.063	16.9	268	0.51	22.8	164	23.6	224	−0.24	7.5	74	572	3
IES-027	33.9	4.88	28.7	2.58	0.174	0.015	13.6	907	–	32.4	154	18.3	213	−2.93	8	8	373	1
IES-028	44.9	3.38	16.4	2.79	0.188	0.041	13.7	334	0.23	23.8	147	25.6	206	−0.45	7.2	33	298	4
IES-029	14.9	3.76	9.77	2.15	0.098	–	1.9	253*	0.15	9.51	81	31.6	115	−2.08	7.8	1	16	1
IES-030	11.9	2.83	31.3	1.29	0.08	0.057	11.2	196	0.63	24.5	81	51.1	179	−0.41	7.4	17	91	3
IES-032	10.7	2.07	11.3	1.59	0.076	0.015	1.92	128	0.33	3.73	65	21.5	89	−1.18	7.9	9	12	1
IES-033	14.6	0.388	6.19	1.27	0.053	–	0.68	91*	0.34	14.6	42	15.7	76	0.55	7.8	4	8	4
IES-034	20.7	4.48	44.8	4.13	0.108	0.063	19.4	308	0.72	13.6	156	51	239	−0.17	7.7	178	1000	3
IES-037	9.86	0.58	3.54	1.15	0.027	0.011	0.23	21	0.23	3.85	39	13.6	53	−1.85	7.7	2	8.008321	4
IES-038	10.3	0.617	3.74	1.3	0.031	–	0.28	37*	–	4.1	41	13.8	56	−2.75	7.8	2	13.75167	4
IES-039	9.25	0.574	7.06	0.925	0.026	0.022	0.44	20	0.25	5.49	41	14.7	60	0.46	7.3	3	10.40712	1
IES-040	22.3	4.97	18.1	2.75	0.114	0.044	4.51	103	0.98	4.48	129	23	146	−0.42	7.2	2	23.49204	1
IES-041	32.9	8.45	18	1.84	0.204	–	2.25	300*	0.1	2.82	191	33.4	196	−1.65	7.1	2	26.11947	1
IES-042	29.7	1.71	10.1	1.79	0.129	0.019	1.87	98	0.51	15.2	106	18	133	−0.99	7.7	15.5235	76.2917	4
IES-043	34.7	2.43	12.4	1.96	0.164	0.017	2.43	143	0.44	12.5	127	22.3	153	1.68	7.4	14	113.681	4

* 0.075 or 75% of the detection limit was used for calculating Cl^{-}/Br^{-} with Br-concentrations below the detection limit (0.1 mg/L).

Group 2 and Group 3 fall below or at the minimum extent of the bounded region. Group 1, which is interpreted to consist of springs weathering granitic plutonic rocks, is predominately in excess of the bounded region (Fig. 11C), with an average Ca^{2+}/Na^{+} molar ratio of 0.72 and a range from 0.38–1.05. Ca^{2+}/Na^{+} molar ratios for Group 4 range from 1.35–1.69 with an average of 1.57 and are far in excess of the bounded region.

The relationship between dominant anions (HCO_3^{-} and SO_4^{2-}) and cations (Ca^{2+} and Mg^{2+}) is shown in Fig. 11D. All samples fall below the equiline representing a 1:1 balance between carbonate weathering (above the line) and silicate weathering (below the line). Group 4 spring waters plot closest to the equiline while Group 3 spring waters plot furthest away. Fig. 11E and F are adapted from Pretti and Stewart (2002) and show mol % for dissolved SiO_2 and Na^{+} relative to Ca^{2+}. Predicted ratios based on the weathering of plagioclase to kaolinite, plagioclase to smectite, and calcite dissolution in equilibrium with plagioclase to smectite weathering are shown as three reference lines in Fig. 11E. Fig. 11F elaborates on the point illustrated with Fig. 11C: 1) The majority of Group 1 waters would need to weather plagioclase with An above the average range for Owens Valley granitoids (An_{28}-An_{36}) to create the observed Ca^{2+}/Na^{+} ratios and 2) the majority of Group 4 waters would need to weather An > An_{50} to create the observed Ca^{2+}/Na^{+} ratios, indicating that there is a calcium source in addition to disseminated calcite. Modal analyses (Table 1) indicate that plutons with average plagioclase compositions of An_{50} or greater are not present in Owens Valley with the exception of mafic plutonic masses (An_{30}-An_{70}) which are not found in the recharge area of Group 4 waters.

The majority of Owens Valley mountain front spring waters ($n = 16$) have Cl^{-}/Br^{-} ratios ranging from (37–300) and are in the range of dilute to moderately evolved groundwaters ($Cl^{-}/Br^{-} \leq 300$) (Danskin, 1998). Two springs, IES-028 and IES-034, are just above this threshold with ratios of 334 and 308, respectively. Two other springs show clear contributions from additional, non-meteoric sources of chloride and have Cl^{-}/Br^{-} ratios >900. These springs, whose local names may be an indicator of their outlier status, are Boron Springs A (IES-025) and Boron Springs B (IES-027). The linear trend observed when Cl^{-}/Br^{-} is plotted against $[Cl^{-}]$ suggests that chloride in being acquired conservatively for most spring waters (Fig. 11G). Lithium and boron concentrations in spring waters, both of which are indicators of geothermal circulation, are strongly correlated in spring waters $R^2 = 0.97$. One spring (IES-024, Hogback Ck. A) falls significantly below this trend line and acquires more lithium versus boron. IES-027 (Boron Spring A) acquires significantly more boron versus lithium compared with other spring waters.

4.6. Geochemistry and noble gases as indicators of circulation and flowpath length

Twelve of the Owens Valley springs yielded unstripped noble gas samples. $^3He/^4He$ ratios normalized to the $^3He/^4He$ ratio of air (R/R_a) range from 0.31 to 1.04 for Owens Valley mountain front spring waters, with an average ratio of 0.82. Four of the 12 springs with unstripped noble gas samples have ratios below 0.7, indicating a significant amount of interaction with subsurface additions of helium. One sample, IES-029, which emerges near Red Mountain and the Big Pine Volcanic field, has the highest R/R_a of 1.04 and is indicative of a potential geogenic ^3He contribution as the majority of He is terrigenic (Table 6). Lower values of R/R_a are related to increasing discharge temperature (Fig. 12A) and increases in the modeled values of terrigenic ^4He (Fig. 12B) derived from Noble90. These trends are stronger without outlier samples (e.g., IES-029). Lower R/R_a is also related to increasing concentrations of geothermal circulation indicators (e.g., Li; Fig. 12C) and overall geochemical evolution as represented by TDS concentrations (Fig. 12D). These trends with R/R_a and weathering derived solutes display a tendency towards separating by geochemical group.

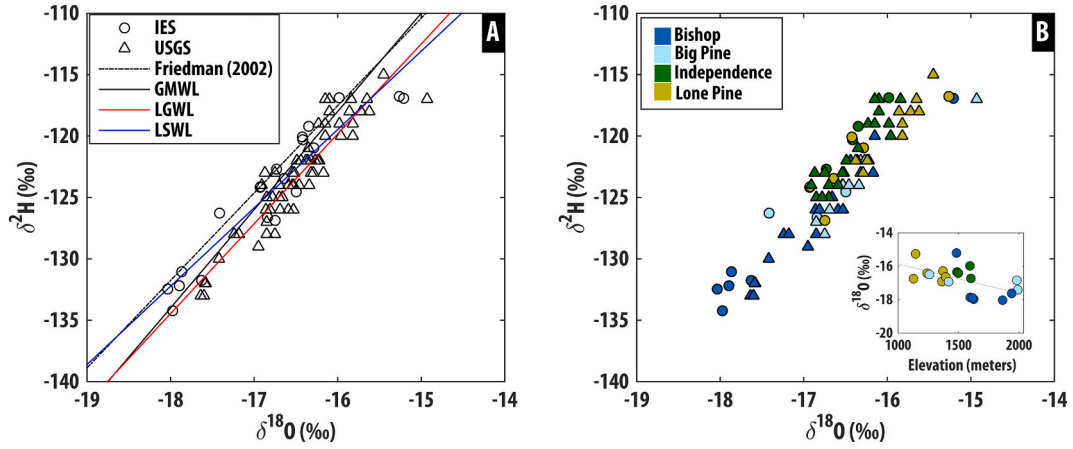

Fig. 6. Dual isotope plots showing $\delta^{18}O$ versus $\delta^{2}H$ for spring waters from this study (IES) and Owens Valley spring and well waters from the USGS Water Quality Portal (USGS). IES springs are shown in the circles and USGS waters are shown in the triangles. A) Waters from both datasets are plotted with four different reference lines; 1) a local meteoric water line from Friedman et al. (2002) (dashed black line), 2) the global meteoric water line (GMWL) from Craig (1961), 3) a local groundwater line (LGWL) fitted to USGS samples, and 4) a local spring water line fitted to IES samples. B) Dual isotope plot ($\delta^{18}O$ versus $\delta^{2}H$) with USGS and IES samples colored by geographic region. Inset plot shows spring elevation versus $\delta^{18}O$ for IES springs.

Table 5
Stable isotope data.

Sample ID	$\delta^{2}H$	$\delta^{18}O$	d_{excess}	$^{87}Sr/^{86}Sr$
	±0.83	±0.08	(‰)	±0.00005
IES-021	−120.1	−16.42	11.3	0.70809
IES-022	−124.1	−16.92	11.3	0.70812
IES-023	−121.0	−16.29	9.3	0.70832
IES-024	−123.5	−16.64	9.7	0.70805
IES-025	−126.9	−16.75	7.1	0.70856
IES-026	−116.8	−15.26	5.3	0.70943
IES-027	−122.7	−16.73	11.2	0.70924
IES-028	−116.9	−15.98	11.0	0.70867
IES-029	−124.2	−16.93	11.3	0.70843
IES-030	−124.5	−16.50	7.4	0.71234
IES-032	−131.8	−17.63	9.3	0.70901
IES-033	−131.0	−17.87	11.9	0.71001
IES-034	−116.9	−15.21	4.7	0.70882
IES-037	−134.2	−17.97	9.6	0.70933
IES-038	−132.2	−17.90	11.0	0.70928
IES-039	−132.5	−18.03	11.8	0.70913
IES-040	−126.3	−17.41	13.0	0.70729
IES-041	−126.6	−16.84	8.1	0.70778
IES-042	−119.2	−16.35	11.6	0.70879
IES-043	−120.3	−16.42	11.0	0.70896

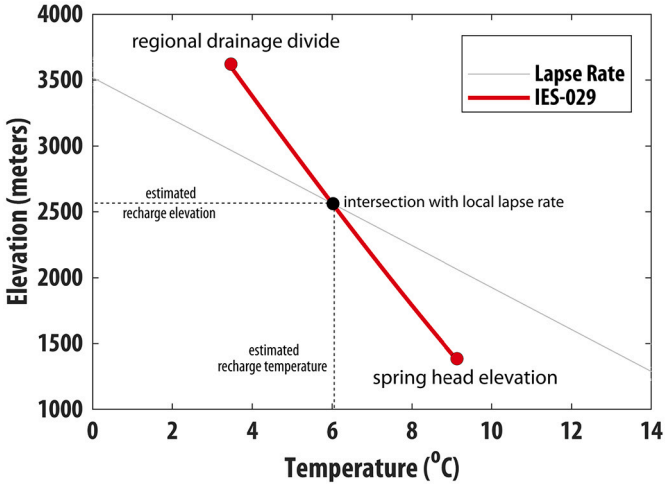

Fig. 7. Shows recharge temperature solved at 100 m increments from the elevation of the spring emergence to the local high elevation point for an example spring, IES-029. The intersection with the environmental lapse rate can be used to estimate recharge elevation (H) and calculate recharge temperature when H is unknown as shown by Zuber et al. (1995), Aeschbach-Hertig et al. (1999), Doyle et al. (2015), and Peters et al. (2018).

4.7. Inverse geochemical modeling results

Inverse geochemical models were constructed to discern the suite and amount of mineral weathering necessary to create spring water compositions evolving from NADP-derived precipitation chemistry. Model phases and stoichiometries were based on field petrologic data (Table 1). Model inputs including mineral forcing constraints and favorable precipitating clays were determined from saturation indices and stability diagrams. Hydrochemically realistic models with a minimal number of solutions were created for 18 of the 20 springs. Two of the springs, IES-026 and IES-030 were not able to be modeled successfully. IES-026 inherits some part of its geochemical composition from the Owens River or leakage along the LAA. IES-030 has an anomalously high $^{87}Sr/^{86}Sr$ ratio compared to Sierra Nevada plutonic rocks and its general chemistry composition cannot be explained by weathering through the surrounding geology. Local masses of felsic dikes and masses in the area, chiefly aplite, pegmatite, and alaskite, with unconstrained petrologic data may explain the inability to model IES-030 successfully.

For the successfully modeled springs, CO_2, gypsum, halite, calcite, K-spar, plagioclase, and biotite or hornblende are present as dissolving phases in each model solution (i.e., solutions are not found without including these phases). Either SiO_2 and kaolinite or ca-montmorillonite are also required to precipitate in every model (Fig. 13). Model results are highly influenced by the Ca^{2+} to Na^{+} ratio in plagioclase. In some cases where the ratio is not well constrained from the petrologic data, multiple model results were considered across a suite of plagioclase compositions. Average model mole transfers are shown in Fig. 13. The majority of spring waters only have one viable model. In contrast with Rademacher et al. (2001) and Blumhagen and Clark (2008), viable models for all springs require calcite as a phase to balance however mole transfer amounts are typically small, except for Group 4 waters. Group 4 waters require large mole transfers of calcite, in terms of percent contribution, to successfully model their geochemical compositions (Fig. 13). IES-025, the basin spring, requires large amounts of halite and gypsum dissolution for the model to successfully balance. This inverse

Table 6
Raw noble gas data and calculated parameters from Noble90.

	Raw Data						Calculated parameters					
Sample ID	Ar total	Ne total	Kr total	Xe total	^{4}He	R/R$_a$	Recharge Elevation[a]	Recharge Temp[b]	Recharge Temp err[b]	^{4}He$_{terr}$ [b]	Chi^2 [b]	Excess Air [b]
	(ccSTP/g)	(ccSTP/g)	(ccSTP/g)	(ccSTP/g)	(ccSTP/g)		(meters)	(°C)	(+-°C)	(ccSTP/g)		(% Ne)
IES-021	3.17E-04	1.65E-07	7.51E-08	1.11E-08	4.71E-08	0.807	2500	6.1	0.9	9.07E-09	0.02	8.0
IES-022	–	–	–	–	–	–	–	–	–	–	–	–
IES-023	–	–	–	–	–	–	–	–	–	–	–	–
IES-024	3.13E-04	1.67E-07	7.17E-08	1.04E-08	1.89E-07	0.308	1900	7.7	1.0	1.50E-07	0.26	11.6
IES-025	–	–	–	–	–	–	–	–	–	–	–	–
IES-026	3.38E-04	1.56E-07	8.23E-08	1.21E-08	3.69E-08	0.978	3400	3.2	0.9	1.86E-09	0.36	0
IES-027	3.16E-04	1.50E-07	7.21E-08	1.02E-08	5.51E-08	0.691	1900	7.4	1.0	2.06E-08	1.60	0.6
IES-028	3.14E-04	1.44E-07	7.64E-08	1.18E-08	2.63E-07	0.469	3000	5.0	0.9	2.28E-07	2.50	0
IES-029	3.70E-04	1.92E-07	8.86E-08	1.25E-08	1.46E-07	1.036	2500[c]	2.3	1.0	1.01E-07	1.26	21.4
IES-030	–	–	–	–	–	–	–	–	–	–	–	–
IES-032	–	–	–	–	–	–	–	–	–	–	–	–
IES-033[*]	–	–	–	–	–	–	–	–	–	–	–	–
IES-034	1.42E-04	1.17E-07	2.59E-08	3.36E-09	7.90E-08	0.595	–	48.8[d]	1.9	4.73E-08	2.04	8.8
IES-037	3.35E-04	1.58E-07	8.19E-08	1.21E-08	3.68E-08	0.986	3400	3.4	0.9	1.54E-09	0.16	0.5
IES-038	–	–	–	–	–	–	–	–	–	–	–	–
IES-039	–	–	–	–	–	–	–	–	–	–	–	–
IES-040	3.35E-04	1.73E-07	7.99E-08	1.26E-08	4.10E-08	0.984	3300	3.5	0.9	1.70E-09	0.49	9.5
IES-041	3.53E-04	1.70E-07	8.86E-08	1.29E-08	4.09E-08	0.972	3000[c]	1.6	1.0	2.74E-09	0.46	6.0
IES-042	3.38E-04	1.66E-07	8.13E-08	1.21E-08	5.17E-08	0.879	3300	3.6	1.0	1.41E-08	0.08	5.9
IES-043	3.33E-04	1.74E-07	8.16E-08	1.21E-08	5.09E-08	0.878	3200	3.9	1.0	1.11E-08	0.06	10.9

[*] Noble gas sampled collected but stripped.
[a] Calculated with the ELR intersection method.
[b] Calculated assuming a median recharge elevation of 2600 m.
[c] Calculated using partial re-equilibration (PR) rather than closed system equilibration.
[d] Recharge temperature elevated, however sample does not appear to be stripped.

modeling result is supported by the elevated spring water Cl-/Br- (1497).

4.8. Strontium ionic relationships and $^{87}Sr/^{86}Sr$

Spring Sr^{2+} concentrations show a positive correlation relationship with Ca^{2+}, especially when separated out by geochemical grouping (Fig. 14A). Group 1 waters, which source flow from the Mount Whitney intrusive suite in the Lone Pine AOI, show a diverging geochemical trend and acquire more Sr^{2+} per mol of Ca^{2+} compared to other Group 1 waters (Fig. 14A).

For 19 out of the 20 springs, $^{87}Sr/^{86}Sr$ ratios fall in a range from 0.70729 to 0.71000. Most values are slightly above the expected window for eastern Sierra Mesozoic granitoids (0.70600–0.70800) (Chen and Tilton, 1991; Hirt, 2007; Chapman et al., 2015). One spring, IES-030, has an anomalously high $^{87}Sr/^{86}Sr$ ratio (0.71234) (not shown in Fig. 14) in comparison to other spring waters and cannot be reconciled based on whole rock strontium ratios of the surrounding geology in the Warren Bench area. It is possible that this elevated ratio could be a result of weathering felsic dikes and masses in the area, chiefly aplite, pegmatite, and alaskite. Not considering the outlier value (IES-030), average $^{87}Sr/^{86}Sr$ ratio for the geochemical groups are 0.70835, 0.70856, 0.70912, and 0.70927 for Groups 1–4, respectively. The average $^{87}Sr/^{86}Sr$ ratio for Group 4 waters plots closest to the expected range for Penn-Permian roof pendants (>0.710) based on whole rock values (Kistler and Peterman, 1973; Goff et al., 1991) and surface waters sourcing areas with roof pendants (Pretti and Stewart, 2002). This $^{87}Sr/^{86}Sr$ range is wide and highly variable even among different lithologic facies within the same roof pendant septa.

Mesozoic granitoid leachates have a narrow range of $^{87}Sr/^{86}Sr$ ratios (0.708462–708,879) with an average isotopic value of 0.708598. These values are elevated when compared to expected whole rock $^{87}Sr/^{86}Sr$ ratios for Mesozoic granitoids, however, these leachate values more closely match the ratios for spring waters compared with the whole rock values. One sample was leached from the Bishop Tuff and this yielded a slightly higher $^{87}Sr/^{86}Sr$ ratio of 0.70948. This value closely matches the $^{87}Sr/^{86}Sr$ ratio of Birchim Cyn. Spring B (IES-034), which emerges directly out of the Bishop Tuff.

Results from general chemistry and inverse geochemical modeling are combined with $^{87}Sr/^{86}Sr$ ratios for leachates and spring waters. With the exception of IES-30, Owens Valley spring waters show a systematic trend of decreasing Ca^{2+}/Sr^{2+} (Fig. 14B) as a function of decreasing $^{87}Sr/^{86}Sr$. Blum et al. (1998) utilized Ca/Sr ratios to differentiate carbonate versus silicate weathering in a watershed with Ca sources from silicates, marble, and vein calcite. Group 4 waters, interpreted to be weathering a combination of Sierra Nevada granitoids and Penn-Permian roof pendants, fall within the Ca^{2+}/Sr^{2+} range of 200–400 and have 6 of the 7 highest Ca/Sr ratios. While Groups 1, 2, and 3 show no trend in strontium isotope evolution as carbonate weathering increases as a function of overall weathering (carbonate/ (plagioclase + carbonate)), Group 4 waters show a linear decrease in $^{87}Sr/^{86}Sr$ (Fig. 14C).

The amount of dissolved silica in solution increases with decreasing elevation in silicate watersheds (Drever and Zobrist, 1992) and thus can be inferred to represent residence time. This relationship is also evident in the Owens Valley springs (Fig. 14F). Similarly, inverse model results like the amount of plagioclase weathered or kaolinite precipitated are informative in understanding how mineral weathering affects $^{87}Sr/^{86}Sr$. Spring waters in all geochemical groups show a systematic decrease in $^{87}Sr/^{86}Sr$ as a function of plagioclase weathering (Fig. 14D), amount of clay mineral formation (Fig. 14E), and silicate dissolution (Fig. 14F). As each of these metrics increase, Owens Valley spring waters converge towards the whole rock $^{87}Sr/^{86}Sr$ range for Mesozoic granitoids in Owens Valley and away from rock leaching values.

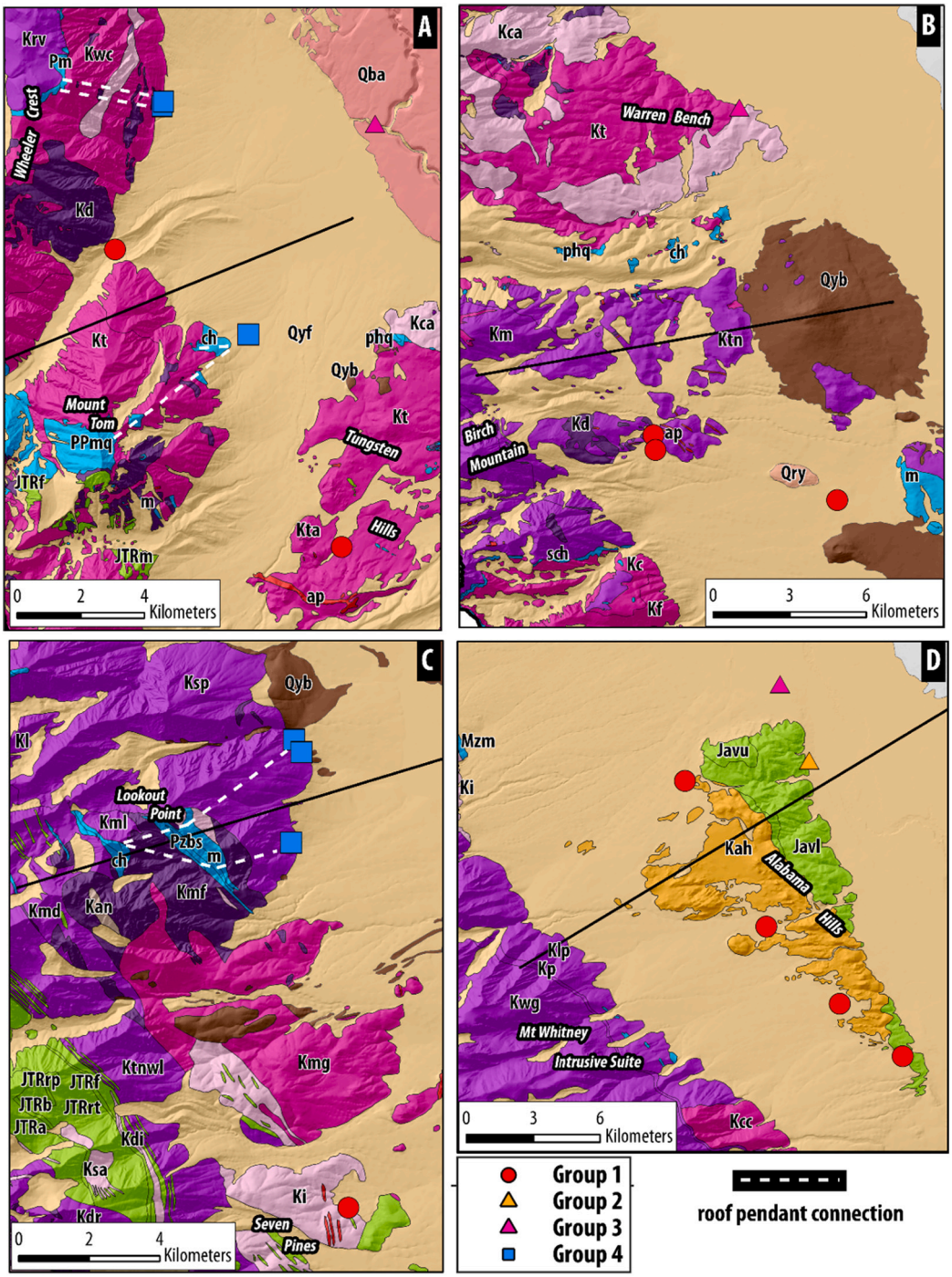

Fig. 8. Zoomed-in geologic maps showing geologic AOIs, springs symbolized by geochemical grouping, and hypothesized connections (white dashed lines) to Group 4 springs (blue squares) from Paleozoic metasedimentary roof pendants (blue geologic units). A) Bishop AOI with Wheeler Crest, Mount Tom, Tungsten Hills subregions shown, B) Big Pine AOI with Warren Bench and Birch Mountain subregions shown, C) Independence AOI with Lookout Point and Seven Pines subregions show, and D) Lone Pine AOI with Mt. Whitney Intrusive Suite and Alabama Hills subregions shown. (For interpretation of the references to colour in this figure legend, the reader is referred to the web version of this article.)

5. Discussion

5.1. *Extending Feth et al. (1964) and Garrels and Mackenzie (1967) to the mountain front*

Geochemical data (e.g., temperature and major ions) of ephemeral and perennial mountain block springs from Feth et al. (1964) combined with results from this study provide a means to investigate how increasing groundwater flowpath length and inferred differences in circulation depth influence spring geochemical composition from local to intermediate spatial scales. The positive correlation between spring discharge temperature and elevation (Fig. (4A) suggests that higher elevation springs are sourcing shorter, more local scale flowpaths and lower elevation springs are sourcing longer, deeper flowpaths. In addition, mountain front springs with higher spring discharge temperatures have a greater positive offset from the ELR. This assertion is also supported by the noble gas data; increasing mountain front spring discharge temperatures are associated with decreasing R/R_A. The majority of mountain front springs fall above the calculated local annual ELR and thus can be interpreted to potentially indicate geothermal heating with rock units whose temperature is modified by the geothermal gradient as a result of groundwater circulation in the mountain block. However, none of these springs have temperatures that are sufficiently elevated to be classified as warm or hot springs indicative of deep circulation and/or limited thermal mixing. Increases in spring discharge temperature from high elevation local-scale springs (e.g., > 1930 mamsl) to mountain

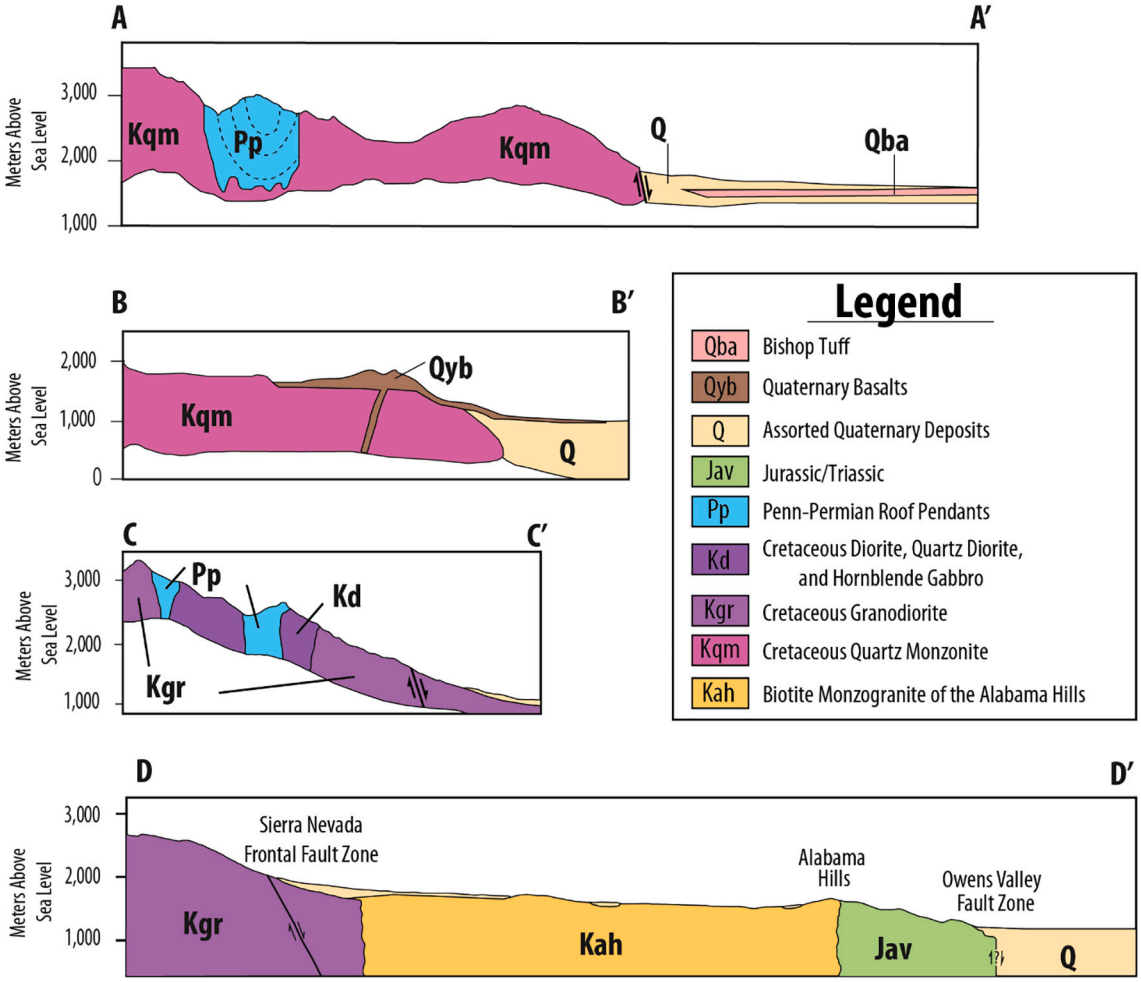

Fig. 9. Simplified geologic cross sections across transects outlined in Fig. 3. The cross sections are described as follows: A) A transect across the Pine Creek Pendant into Round Valley, CA. Cross section adapted from Bateman et al. (1965), B) A transect through the Big Pine AOI from north of Birch Mountain to Crater Mountain. Cross section adapted from Bateman et al. (1965), C) Simplified cross section though metasedimentary roof septa and Spook Pluton near Independence, CA. IES-028, IES-042, and IES-043 likely source units featured in this cross section. Cross section adapted from Moore (1963), D) Simplified cross section of the geologic AOI near Lone Pine, CA. Springs IES-021, IES-022, IES-023, IES-024 are likely influenced by the Mount Whitney Intrusive Suite and Alabama Hills biotite monzogranite. Cross section adapted from Stone et al. (2000).

front and basin springs provide evidence for increasing groundwater circulation in the mountain block. Ephemeral and perennial mountain block springs have lower average spring discharge temperatures and have a higher proportion of samples that fall below the local ELR compared with the mountain front springs. The statistically significant spring elevation versus discharge temperature trends observed when comparing (1) all spring data and (2) only the mountain front springs imply that the temperature increase is as a result of geothermal heating as intermediate scale flowpaths circulate through the mountain block.

Increases in major ion concentrations as a function of specific conductivity and noble gas indicators of circulation for the mountain front spring samples are best represented by linear relationships. In comparison, increases in major ion concentrations as a function of specific conductivity are best represented by power-law trends when the ephemeral and perennial spring data are included. These trends are strongest for calcium and bicarbonate and are weaker for classic silicate weathering products like sodium, potassium, and silica. Our results suggest that the weathering of calcite sustains geochemical evolution at intermediate flowpath lengths through the mountain block in the eastern Sierra Nevada. When the spatial scale of analysis is extended to include the basin spring, power-law trends of solutes likely derived from evaporative concentration or the dissolution of more easily weatherable alluvial material best describe the weathering trends (Fig. 5). Previous studies have found that there are kinetic limits on silicate weathering with increasing scale (e.g., Winnick and Maher, 2018), and that these limits have implications for global chemical weathering rates. Therefore, the finding of sustained chemical weathering in mountain block aquifers is critical to understand and constrain further.

5.2. *Spring sourcing and contributing areas of mountain front springs*

Delineating contributing areas to springs is a challenge in hydrogeology because groundwater divides are inherently different from topographic surface waters divides (Frisbee et al., 2013a, 2013b). This is complicated by the fact that these contributing areas are in reality 3-dimensional volumes rather than 2-dimensional areas with sometimes negligible depths. To understand the dominant controls on geochemical evolution with increased spatial scale and residence time, it is first necessary to determine some conceptual bounds on the extent of spring contributing areas in order to identify likely host aquifers. The Sierra Nevada batholith is both long and wide, and it is unknown how fracture porosity and interconnectivity change with depth in the bedrock. Therefore, it is unknown how fracture networks route groundwater flow from high elevation recharge areas to intermediate and regional-scale springs. However, stable isotopes and noble gas recharge parameters can inform conceptual models for spring contributing area (e.g., Miller

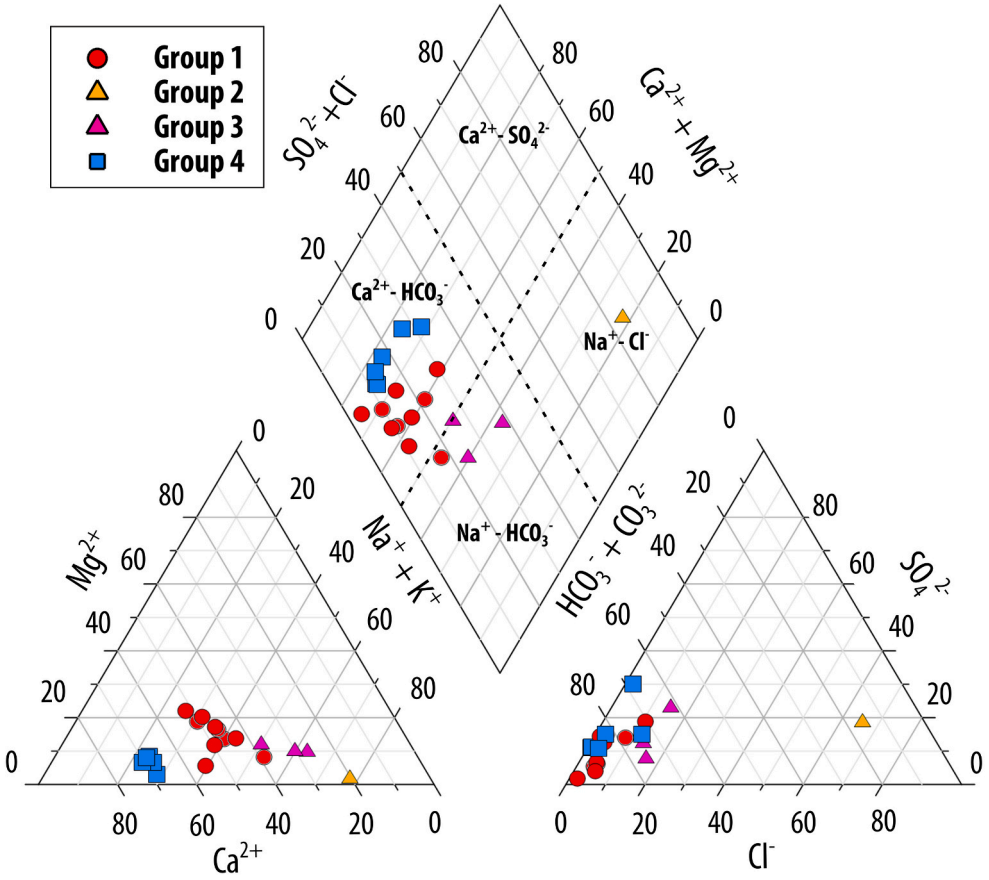

Fig. 10. Piper diagram showing geochemical compositions of spring waters. Springs are symbolized by geochemical grouping.

et al., 2017; Zhang, 2021). In this study we apply these tools to constrain contributing areas for springs emerging at the base of the eastern Sierra Nevada.

δ^2H and $\delta^{18}O$ values from the USGS NWIS and from this study display a dependence on geographic location within Owens Valley (Fig. 6B). Isotopically light samples are found in the Round Valley area west of Bishop, CA and near Big Pine, CA in the northern part of Owens Valley. These samples correspond to isotopically depleted areas in the eastern Sierra identified by Friedman and Smith (1972). Isotopically enriched samples are found in southern portions of the valley (near Independence, CA and Lone Pine, CA) and at lower-lying basin locations (IES-026 and IES-034). High resolution deuterium contours of eastern Sierra Nevada winter precipitation from Friedman and Smith (1972) support an interpretation that mountain front Owens Valley spring waters are sourcing the majority of their recharge from east of the Sierra Nevada drainage divide, otherwise deuterium contents would likely be more depleted. These combined results support an interpretation that recharge to springs is locally sourced (east of the Sierra Nevada drainage divide) and relatively geographically isolated by region within Owens Valley.

The strong influence of geography makes it challenging for stable isotopes to serve as recharge elevation tracers at a regional scale. Although δ^2H and $\delta^{18}O$ are weakly correlated with spring emergence elevation (Fig. 6B), these relationships are not strong enough to derive potential recharge elevations as illustrated by James et al. (2000). However, δ^2H and $\delta^{18}O$ still have utility in distinguishing sources and geographic location of recharge. δ^2H and $\delta^{18}O$ values from 18 springs, including the basinal brine (IES-025), are consistent with snowmelt-derived recharge from high elevation areas eastern Sierra Nevada. Expected $\delta^{18}O$ values for winter precipitation at mid to high elevations range between −15 to −19‰ in the northern half of the valley and between $\delta^{18}O$ to −17‰ in the southern half of the valley (Fig. B.3). Low-lying basin and alluvial areas have winter $\delta^{18}O > -14$‰. The springs in this study have $\delta^{18}O$ values ranging from −18.0 to −15.2‰ that are more isotopically depleted moving northward. Dual isotope and d_{excess} values suggest that IES-026 and IES-034, both of which lie towards the geographic center of the basin, are not primarily sourcing snowmelt derived recharge and thus are probably not indicative of flowpaths with increased scale from high elevation areas (Table 5). These springs are likely discharging recharge from lower elevations or recharge with a higher percentage derived from rainfall as opposed to snowmelt.

Noble gas recharge elevations derived from the ELR method indicate that the majority of recharge is occurring at elevations between 1900 and 3400 mamsl (Table 6). This range of elevations is found directly upgradient for most of the springs. Noble gas recharge temperatures, both from the ELR method (avg. 4.0 °C) and the median elevation method (avg. 4.3 °C) indicate that mountain front springs in Owens Valley source cold recharge, likely snowmelt. These results suggest that the water discharging from the mountain front springs was recharged at a considerably higher elevation than the spring emergence zones and provides support for the assumed flowpaths and flowthrough geologic units. Springs further away from the drainage divide like those in the Alabama Hills (IES-021 & IES-024) or near Red Mountain (IES-029) may have greater recharge accumulation zones (e.g., losing reaches of mountain-draining streams in the alluvial aquifer) and thus decreased recharge elevations and increased recharge temperatures. These metrics serve as an important baseline for evaluating how these springs will respond to changes in recharge due to climate change if the snowline decreases in elevation. The coupling of these noble gas results with interpretations from δ^2H and $\delta^{18}O$ (i.e., recharge supporting springs is geographically limited) and spring discharge temperatures leads us to infer that the plutons and geologic units upgradient of springs are the

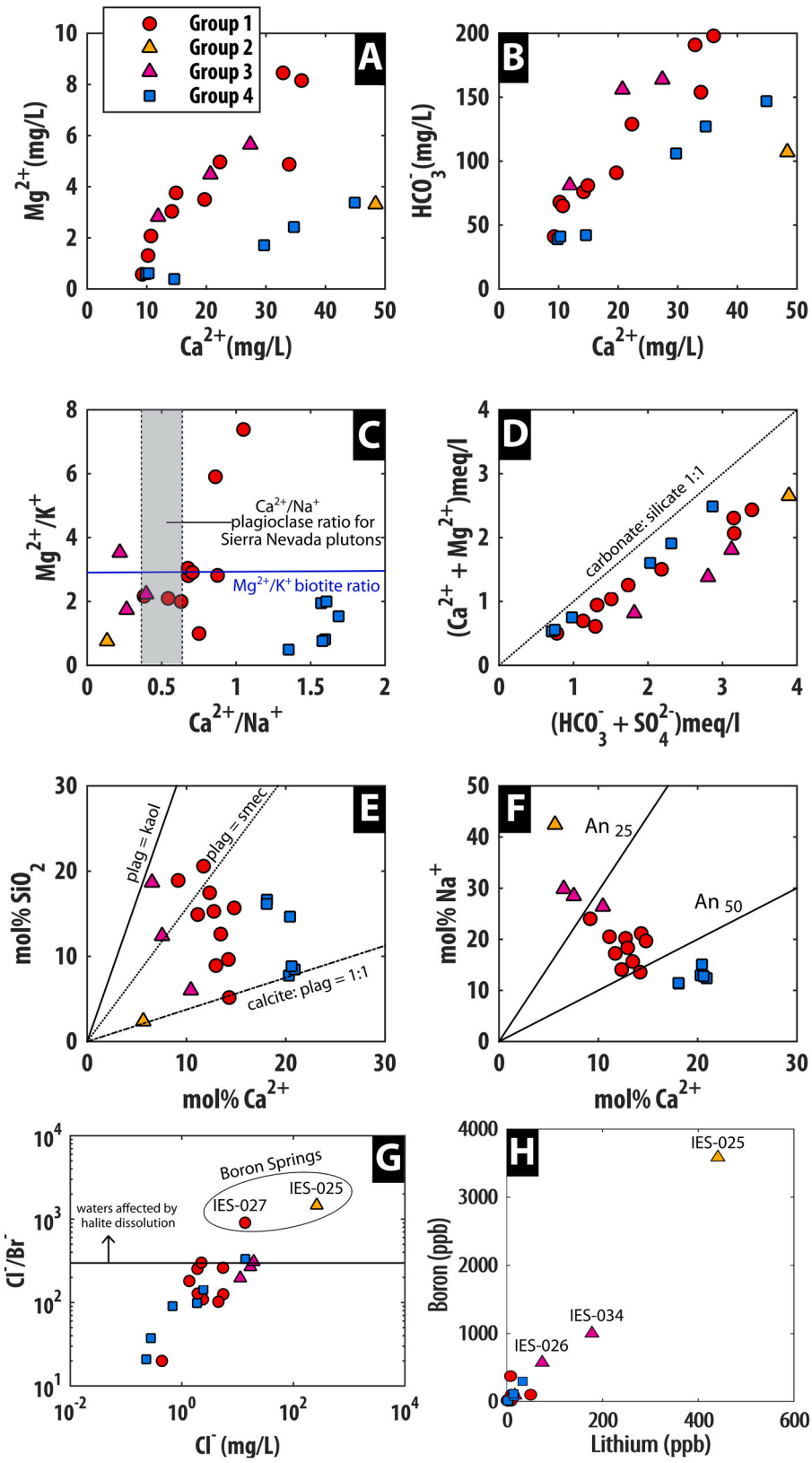

Fig. 11. Geochemical relationships among weathering derived solutes for Owens Valley spring waters. Springs are symbolized by geochemical grouping. A) Relationship between calcium and magnesium ion concentrations in sampled spring waters. Springs are well below the 1:1 Mg^{2+}: Ca^{2+} line representative of hornblende weathering. B) Relationship between calcium and bicarbonate ion concentrations C) Relationship between magnesium/potassium ion ratios and calcium/sodium ion ratios in sampled spring waters. The trend line expected for biotite weathering for Mg^{2+}/K^{+} (~3) is shown by the blue line. The expected Ca^{2+}/Na^{+} weathering ratio for granitic plutons in Owens Valley (Table 1) (An_{28}-An_{36}) is bounded for reference in the grey box. D) Relationship between dominant anions (HCO_3^- and SO_4^{2-} meq/L) and cations (Ca^{2+} and Mg^{2+} meq/L). All samples fall below the 1:1 reference line indicative of equal contributions from carbonate and silicate weathering. Group 4 springs lie the closest to the 1:1 line. E) Relationship between mol % SiO_2 and mol % Ca. Reference lines for predicted weathering trends are shown for 1) calcite dissolution and plagioclase to smectite weathering in a 1:1 ratio, 2) plagioclase to smectite weathering, and 3) plagioclase to kaolinite weathering. F) Relationship between mol % Ca and mol % Na. Predicted weathering trends for An_{25} and An_{45} plagioclase are shown. Plots E & F adapted from Pretti and Stewart (2002). G) Relationship between Cl^- concentration and Cl^-/Br^- used to assess the sources of Cl in spring waters. Horizontal line at Cl^-/Br^- = 300 denotes the cutoff between waters affected by sources other than meteoric chloride. F) Relationship between trace element indicators of groundwater circulation Li and B in spring waters. (For interpretation of the references to colour in this figure legend, the reader is referred to the web version of this article.)

primary aquifers supplying springflow. Our results suggest that noble gas recharge parameters combined with water stable isotopes can be used to infer the approximate extent of recharge and geologic units likely contributing to springflow.

5.3. Factors controlling the chemical compositions of mountain front springs

5.3.1. The effect of geologic heterogeneity

Local-scale flowpath distributions typically capture a limited set of

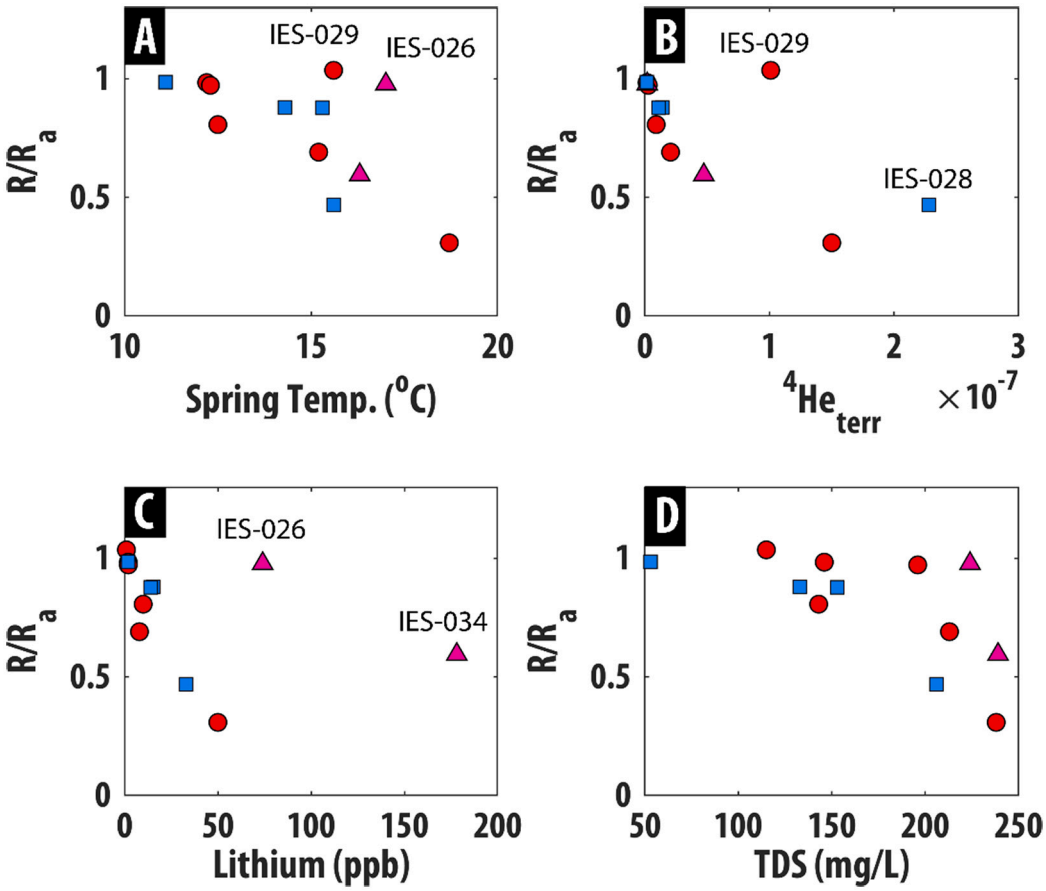

Fig. 12. Relationships with geochemistry analytes and noble gas indictors of groundwater circulation and flowpath length. Springs are symbolized by spring geochemical groupings. A) Spring temperature versus the $^{3}He/^{4}He$ ratio normalized to the $^{3}He/^{4}He$ ratio of air (R/R_a). B) Terrigenic ^{4}He accumulation in spring waters versus R/R_a. C) Lithium concentrations versus R/R_a. D) Total dissolved solids (TDS) versus R/R_a.

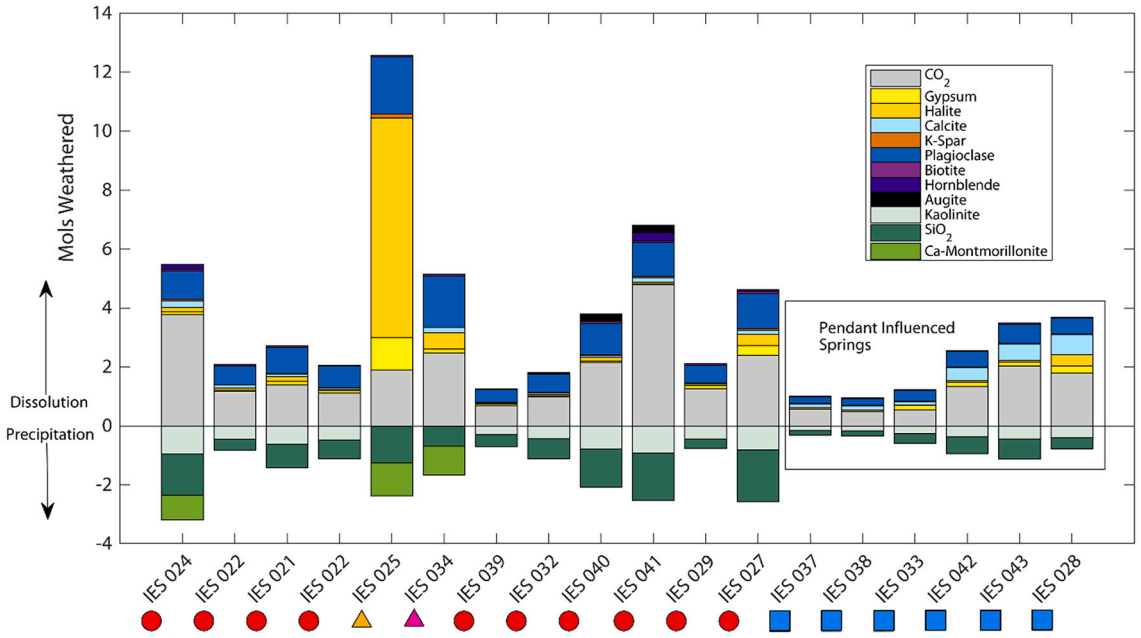

Fig. 13. Results from NETPATH inverse geochemical modeling from NADP precipitation to spring geochemical compositions. Springs are symbolized on the x-axis by their geochemical group. Positive mole transfers indicate dissolution and negative mol transfers indicate precipitation. In instances where multiple models were found, the average of mole transfers is shown. Successful model solutions do not exist without including calcite in these models. Group 4 springs are indicated by the rectangular bounding box. These springs require large mole transfers (% wise) of calcite to successfully model their geochemical composition.

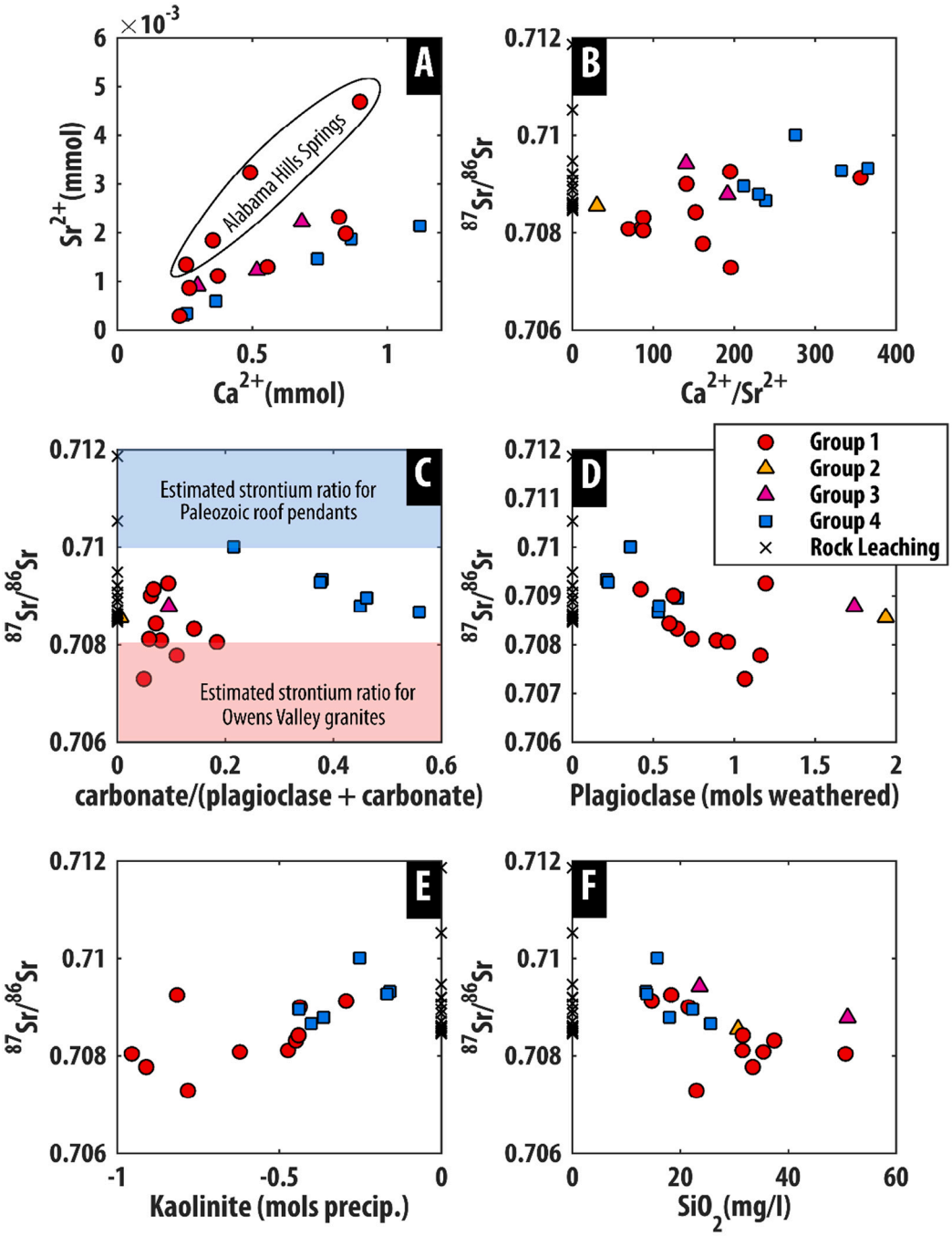

Fig. 14. Relationships with $^{87}Sr/^{86}Sr$, geochemistry, and inverse modeling results for sampled spring waters. Springs are symbolized by geochemical grouping. For plots B—F rock leachate values for Sierra Nevada granitoids are symbolized by the black Xs. A) Relationship between strontium and calcium ion concentrations in sampled spring waters. B) Relationship between $^{87}Sr/^{86}Sr$ and Ca^{2+}/Sr^{2+} ionic ratios in spring waters. C) Mols transfers of carbonate/(plagioclase + carbonate) from inverse geochemical models versus $^{87}Sr/^{86}Sr$. The expected strontium ratio for Owens Valley granites (0.706–0.708) is shown in the pink shaded area. The estimated strontium ratio for Paleozoic roof pendants is shown in the blue shaded area. D) Average plagioclase mol transfer from inverse geochemical models versus $^{87}Sr/^{86}Sr$. E) Average kaolinite mol transfer (negative for precipitation) from inverse geochemical models versus $^{87}Sr/^{86}Sr$. F) Relationship between silica (as SiO_2) and $^{87}Sr/^{86}Sr$. (For interpretation of the references to colour in this figure legend, the reader is referred to the web version of this article.)

geological variability present in bedrock. However, geologic heterogeneity commonly increases with increasing spatial scale and becomes the primary driver of continued geochemical evolution. This relationship is clearly shown by the geochemical patterns exhibited in Owens Valley spring waters where four dominant geochemical groups are identified. These geochemical groups can be attributed to petrologic differences in the aquifer rocks which host groundwater flow paths, based on information gleaned from stable isotopes (spatial extent of recharge) and noble gases (recharge elevation and recharge temperature).

Group 1 spring waters are the most abundant in the study springs and represent groundwater evolving as a result of rock-water interaction with Sierra Nevada plutonic rocks (i.e., alaskite, quartz monzonite, granodiorite, and diorite, quartz diorite, and hornblende gabbro). Group 1 has the most intragroup geochemical variation, which can be attributed to the widely varying petrologic compositions of the plutons supplying flow to springs (Table 1). Subgroups can be identified from within this group that are controlled by local geology. For example, springs downgradient of the Mount Whitney Intrusive Suite emerging from the biotite monzogranite of the Alabama Hills have a separate Sr^{2+} vs Ca^{2+} evolutionary line when compared to other Group 1 waters (Fig. 14C). Springs with $Mg^{2+}/K^{+} \geq 3$ (Fig. 11C) can be explained by upgradient presence of either granodiorites or diorite/quartz diorite/hornblende gabbro (Fig. 8).

The four springs in Groups 2 and 3 are outliers that do not conform to the inferred conceptual model where solute concentrations increase with increasing spatial scale. Group 2 consists of one spring, IES-025, an Na—Cl type seep emerging on the eastern side of the Alabama Hills. This spring is incredibly saline and geochemically evolved compared to other spring waters. Both its geochemistry and landscape placement are indicative of interaction with alluvial material and/or basinal evaporite

deposits. However, its stable isotopic signature is depleted compared to other springs emerging at low elevations (i.e., IES-026 and IES-034), perhaps indicating that basinal brines similar to IES-025 may be sourced from snowmelt recharge at higher elevations. The Group 3 spring waters, which are characterized by a volcanic rock geochemical signature, have numerous lines of evidence supporting a connection between surface water features (Owens River and LAA) and at least two of the three Group 3 waters (IES-026 and IES-034). This evidence includes: 1) enrichment in stable isotope (δ^2H and $\delta^{18}O$) and deuterium excess values, 2) geochemical similarity to surface water features (Bassett et al., 2008), 3) enrichment in lithium concentration, and 4) spatial proximity to surface water features. The chemical compositions at IES-026 and IES-030 cannot be explained by the surrounding geology and do not yield viable inverse model solutions from Netpath-XL.

Springs in Group 4 have a distinctive geochemical evolutionary pathway that we interpret to represent a mixture of roof pendant (e.g., marble, micaceous quartzite, calc-hornfels, and biotite schist) and granitoid dissolution. Evidence for this mixed geochemical signal includes: 1) spatial proximity to Paleozoic metasedimentary roof pendants that are directly upgradient from spring emergences (Fig. 8A & 8C), 2) distinct geochemical compositions compared to springs that are spatially close and in a similar geologic AOIs without roof pendants upgradient in their likely recharge areas (e.g., IES-032 & IES-039), 3) Ca^{2+}/Na^{+} well in excess of 0.4–0.6, and 4) strontium isotope evolution with increasing carbonate influence (Fig. 14C). It is unclear if these roof pendants are areas of enhanced recharge or, as is more likely the case, are areas of preferential weathering and therefore increased solute fluxes. It's unlikely that hornfels-dominated pendants have sufficient permeability to enhance recharge; however, marble may weather more easily and become conducive to recharge. An alternative hypothesis for the excess calcium in Group 4 spring waters is that they are influenced by excess calcium stemming from the weathering of freshly exposed glacial rock (e.g., Blum et al., 1998). IES-32 and IES-39 (Group 4) are both springs located proximally to recently glaciated areas, however these springs do not have roof pendants and have Ca/Na ratios less than 1.0. The source of excess calcite is likely from roof pendant marbles but can also weather from other facies present in roof pendant metamorphic septa such as schists and hornfels.

Our results show that geologic heterogeneity exerts a significant control on geochemical evolution pathways with increased scale in contrast with local-scale flowpath distributions in a geologically homogenous area. The longer these flowpaths are, the greater the observed differences are between the geochemical groups (e.g., Fig. 11). Differences in Group 1 waters, all sourcing flow through Mesozoic granitoids, can be attributed to subtle variations in plutonic composition (i.e., increased abundance of mafic minerals like pyroxene, hornblende percent composition over 5%, etc.). Roof pendant septa, such as the Pine Creek and Bishop Creek roof pendants, exert a control on the geochemistry of springs downgradient (Group 4 waters), even though they are limited in spatial extent in surface area and at depth. Differences in $^{87}Sr/^{86}Sr$ between dilute and evolved waters of different geochemical groups can be attributed to differential mineral weathering. Dilute waters have strontium isotopes that are elevated in comparison to whole rock values due to the preferential weathering of calcite, elevating the Ca^{2+}/Sr^{2+} ratio, and other easily weatherable minerals. For more evolved waters in silicate watersheds, as shown by increases in silica (Fig. 14C), plagioclase dissolution (Fig. 14E), and kaolinite precipitation (Fig. 14F), strontium isotope compositions converge towards the range for whole rock values. Spring water $^{87}Sr/^{86}Sr$ values that are slightly elevated compared to whole rock values may be attributed to the accumulation of dust in snowpack that is incorporated into recharge (e.g., Carling et al., 2020). Distinct geochemical compositions of aridland springs, which serve as keystone ecological features due to the limited presence of surface waters, have implications for the structure and diversity of ecological communities such as groundwater microbes and benthic macroinvertebrates (e.g., Pordel, 2020).

5.3.2. Excess calcium in intermediate scale groundwaters

As previous studies examining silicate weathering have observed, surface and groundwater discharge in granitic terranes exhibit elevated Ca^{2+}/Na^{+} molar ratios over what would be expected solely from the dissolution of plagioclase (White et al., 1999). Plagioclase weathering is the primary source of calcium in granitic watersheds where aeolian deposition is negligible; however, calcium fluxes can be augmented by selective anorthite leaching or dissolution of other silicate phases like hornblende. Excess calcium in the form of calcite was postulated by Garrels and Mackenzie (1967) as a solution to unaccounted weathering products in their inverse geochemical model. White et al. (1999) primarily attributed calcium excesses in granitic watersheds to disseminated calcite and further determined that trace amounts of calcite are ubiquitous in Sierra Nevada granitoids. Trace amounts of calcite in granite massifs can present as disseminated grains in the silicate matrix, calcite replacement of plagioclase, or vein calcite filling fractures (White et al., 1999). While calcite can be a significant source of solutes in granitic watersheds in multiple surface water studies, especially in glaciated catchments where fresh bedrock is readily exposed (Blum et al., 1993; Blum et al., 1998; Pretti and Stewart, 2002), there have been a dearth of studies examining the sources responsible for excess calcium in groundwaters. Here in the present study, for some springs, we see an "excess of excess" calcium as compared to that reported in White et al. (1999).

Mesozoic granitoids (not including diorites) supplying flow to springs in Owens Valley have anorthite compositions ranging from An_{10} to An_{38}, with the majority ranging from An_{28} to An_{36}. Therefore, expected Ca^{2+}/Na^{+} fluxes, assuming no other sources of calcite, should range between 0.4 and 0.6. Group 1 and Group 4 waters identified as sourcing intermediate scale groundwater flowpaths have excess calcium ($Ca^{2+}/Na^{+} > 0.6$) than what would be predicted by An_{28} to An_{36}. In particular, Group 4 waters interpreted to receive some portion of flow through metasedimentary roof pendants have an excess of excess calcium ($Ca^{2+}/Na^{+} > 1.5$) that most likely reflects a combination of contributions from disseminated calcite within the granitoids and calcium weathered from calcite associated with marble, hornfels, and micaceous schists, and from the Pine Creek, Bishop Creek, and Mount Pinchot roof pendants and associated septa.

The results from inverse modeling support the influence of disseminated calcite as a component of the geochemical compositions of all Group 1 and Group 4 spring waters. All springs require calcite as a dissolving phase for models to converge on a solution. Other studies have pointed to weathering of silicate phases like hornblende as potential sources of excess Ca^{2+} (Clow et al., 1997; White et al., 1999). In our case hornblende is included as a phase in all models where it has a documented presence in the modal analyses of the likely flowthrough plutonic rocks. However, it is not critical, unlike the case with calcite, to establishing model solutions and is rarely selected by NETPATH as a phase in viable solutions.

5.4. Implications of this work

Geochemical evolution through the mountain block from the local scale (e.g., Feth et al., 1964) to the intermediate scale of a predominantly silicate terrain is best described by power-law weathering trends. Our results imply that continued geochemical evolution through the mountain block is sustained by the continued weathering of disseminated calcite as dissolved silica concentrations reach saturation and form alumnosilicates. The effect of disseminated calcite is seen in both the springs solely weathering granitic plutonic rocks (Group 1) as well as springs weathering a combination of granitic plutonic rocks and metasedimentary roof pendants and associated septa. In the case of the eastern Sierra Nevada, disseminated calcite within the plutonic rocks is responsible for sustaining chemical reactions. These assertions are

supported by strong weathering relationships with Ca^{2+} and HCO_3^- with specific conductance, inverse geochemical model results, and strontium isotopes. Although disseminated calcite has been previously recognized as a ubiquitous component of granitoid rocks (e.g., White et al., 2005) and as an important contributor of solute fluxes to surface water catchments in granitic terrains (Blum et al., 1998; Horton et al., 1999; Jacobson and Blum, 2000; Jacobson et al., 2002), especially glaciated watersheds, this work provides evidence of the importance of disseminated calcite in sustaining chemical weathering in deep (i.e., intermediate scale) groundwater, and the importance of considering carbonate reactions in the recharge zone, where geology dictates. Prior studies relate the presence of disseminated calcite as an important component of solute weathering fluxes in silicate terrains to a likely overestimation of silicate weathering rates using Sr isotope geochemistry (Blum et al., 1998; Jacobson and Blum, 2000; Jacobson et al., 2002). Understanding global silicate weathering rates is critical for understanding the global carbon cycle (Berner, 1992; Maher and Chamberlain, 2014) and has implications for forecasting the future impacts of anthropogenic CO_2 emissions (Penman et al., 2020). The findings from this work imply that silicate weathering rates in granitic terrain may be further overestimated than previously thought if disseminated calcite is critical in sustaining geochemical evolution with increased flowpath length, especially given our growing understanding of the importance of the contribution of deep groundwater to streamflow in bedrock catchments (e.g., Frisbee et al., 2013a, 2013b).

One of the key findings of Garrels and Mackenzie (1967) is that field metrics, such as electrical conductivity and/or TDS, can be used to infer the spatial scale of flowpaths and groundwater residence times in small headwater catchments dominated by local-scale flowpaths. The results from our study indicate solute geochemistry can be effectively used to understand flowpath length and groundwater circulation at the much larger mountain-front scale and may be related to groundwater residence times at this scale (e.g., Frisbee et al., 2011). There are strong relationships among mountain front spring geochemical compositions and geochemical indicators of groundwater circulation and flowpath length (e.g., spring temperature, R/R_A, strontium isotopic evolution). When the effect of geologic heterogeneity can be minimized, i.e., when only examining springs within individual geochemical groups, these relationships are even stronger. For example, within Group 4 –the springs influenced by silicate weathering of plutonic rocks and Penn-Permian metasedimentary roof pendants– there are strong, systematic increases in geochemical evolution, indicators of gradual geothermal heating (e.g., spring temperature and Li), strontium isotope evolution, and noble gas indicators of circulation (Fig. 15). In an area such as the eastern Sierra Nevada where geologic heterogeneity exerts a control on solute evolution patterns, mole transfers of minerals that are ubiquitous across a study area (i.e., plagioclase and biotite) calculated from inverse geochemical models may provide a more robust metric indicative of geochemical evolution as opposed to TDS or an ion with multiple sources. For example, at the catchment scale, Rademacher et al. (2001) showed strong relationships between residence time and biotite and hornblende weathering in shallow groundwater. Future work at the mountain front, intermediate scale will assess the relationship between simple geochemical metrics (i.e., specific conductance or inverse modeling results) and direct measurements of groundwater residence time at the mountain-front scale.

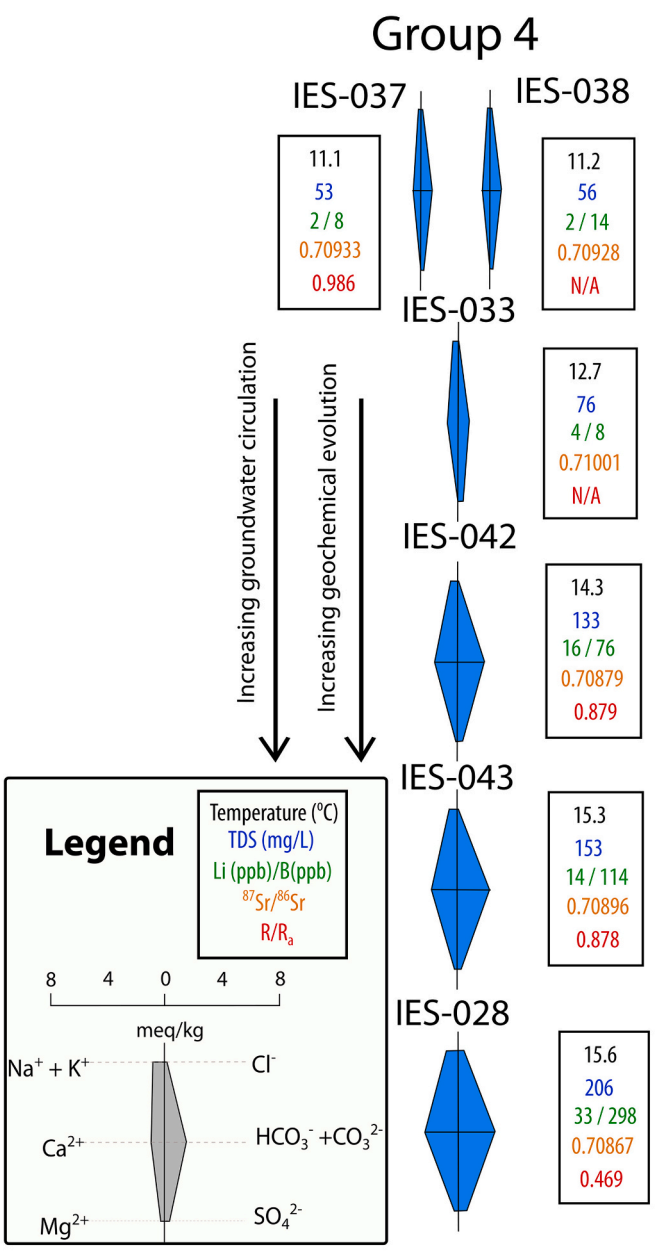

Fig. 15. Stiff diagrams showing geochemical evolution among Group 4 mountain front spring waters. Increasing geochemical evolution generally coincides with increasing temperature, increases in trace element indicators of geothermal circulation (e.g., Li and B), decreasing $^{87}Sr/^{86}Sr$, and decreasing R/R_A.

6. Conclusions

Our results show that geochemical evolution within the mountain block from local to intermediate scales, as evidenced by mountain front springs, follows power-law weathering trends prior to geochemical overprinting and evaporative concentration of solutes in the alluvial basin. A number of other studies have evoked similar power-law relationships with silicate weathering and scale or residence time (e.g., Maher, 2011; Frisbee et al., 2013a, 2013b; Winnick and Maher, 2018).

While silicate weathering reactions dominate geochemical evolution at local scales, the dissolution of disseminated calcite becomes increasingly important for sustaining chemical weathering at longer flowpath lengths. This is true for the case of springs primarily weathering granitic plutons and as well as for springs weathering a combination of granitic plutons and metasedimentary roof pendants. Geochemical solute plots, inverse geochemical models, and strontium isotopes show that disseminated calcite within granitic plutons can be a significant component of solute fluxes out of granitic watersheds, not just in shallow groundwater, surface water, and glaciated catchments, but in intermediate to regional scale groundwater. This result has implications for modeling solute fluxes out of watersheds and potential implications for the global carbon cycle. Additionally, our results show that with increased scale (i.e., groundwater circulation and flowpath length) the principal factor

driving geochemical evolution is geologic heterogeneity. This point is emphasized by the effect of Paleozoic metasedimentary roof pendants, when present in inferred recharge areas, on spring geochemical compositions. However, within geochemical groups, the findings from this work suggest that spring geochemistry can be used to infer flowpath length and groundwater circulation, thereby implying that spring geochemistry can be used to estimate groundwater residence time. Future work will (1) explicitly test whether groundwater geochemistry and simple geochemical measurements (e.g., specific conductance) can be used to serve as proxies for groundwater residence time and (2) the effect of spring geochemistry and groundwater flowpath distribution on spring ecological communities (i.e., microbiology and aquatic ecology).

Funding

Funding for this research was provided by NSF EAR 1516127 and EAR 1516698.

Declaration of Competing Interest

The authors declare that they have no known competing financial interests or personal relationships that could have appeared to influence the work reported in this paper.

Acknowledgements

We thank the permitting agencies: Rosalie Herrera and Kary Schlick (Inyo National Forest) and Jeffrey Nordin (Los Angeles Department of Water and Power). We also thank the research team for field assistance: Brian Hedlund and Ariel Friel (UNLV), Don Sada and John Umek (DRI-Reno), and Khaled Pordel (UNR). We would also like to thank the comments of three anonymous reviewers for greatly improving the quality of this manuscript.

Appendix A. Supplementary data

Supplementary data to this article can be found online at https://doi.org/10.1016/j.chemgeo.2022.120831.

References

Abbott, E.W., 1972. Stratigraphy and petrology of the Mesozoic volcanic rocks of southeastern California, Doctoral dissertation. Rice University.
Aeschbach-Hertig, W., Peeters, F., Beyerle, U., Kipfer, R., 1999. Interpretation of dissolved atmospheric noble gases in natural waters. Water Resour. Res. 35 (9), 2779–2792.
Aeschbach-Hertig, W., Peeters, F., Beyerle, U., Kipfer, R., 2000. Palaeotemperature reconstruction from noble gases in ground water taking into account equilibration with entrapped air. Nature 405 (6790), 1040–1044.
Bassett, R.L., Steinwand, A., Jorat, S., Petersen, C., Jackson, R., 2008. Forensic isotope analysis to refine a hydrologic conceptual model. Groundwater 46 (3), 372–383.
Bateman, P.C., Moore, J.G., 1965. Geologic Map of the Mount Goddard quadrangle. Fresno and Inyo Counties. US Geological Survey Map GQ-429, California. Scale, 1 (62,500).
Bateman, P.C., Pakiser, L.C., Kane, M.F., 1965. Geology and Tungsten Mineralization of the Bishop District, California, with a Section on Gravity Study of Owens Valley and a Section on Seismic Profile (No. 470). US Govt. Print. Off.
Bense, V.F., Gleeson, T., Loveless, S.E., Bour, O., Scibek, J., 2013. Fault zone hydrogeology. Earth Sci. Rev. 127, 171–192.
Berner, R.A., 1992. Weathering, plants, and the long-term carbon cycle. Geochim. Cosmochim. Acta 56 (8), 3225–3231.
Blasch, K.W., Bryson, J.R., 2007. Distinguishing sources of ground water recharge by using δ2H and δ18O. Groundwater 45 (3), 294–308.
Blum, J.D., Erel, Y., Brown, K., 1993. 87Sr/86Sr ratios of Sierra Nevada stream waters: Implications for relative mineral weathering rates. Geochim. Cosmochim. Acta 57 (21–22), 5019–5025.
Blum, J.D., Gazis, C.A., Jacobson, A.D., Page Chamberlain, C., 1998. Carbonate versus silicate weathering in the Raikhot watershed within the High Himalayan Crystalline Series. Geology 26 (5), 411–414.
Blumhagen, E.D., Clark, J.F., 2008. Carbon sources and signals through time in an Alpine groundwater Basin, Sagehen California. Appl. Geochem. 23 (8), 2284–2291.
Bowen, G.J., Revenaugh, J., 2003. Interpolating the isotopic composition of modern meteoric precipitation. Water Resour. Res. 39 (10).
Bowen, G.J., Wassenaar, L.I., Hobson, K.A., 2005. Global application of stable hydrogen and oxygen isotopes to wildlife forensics. Oecologia 143 (3), 337–348.
Carling, G.T., Fernandez, D.P., Rey, K.A., Hale, C.A., Goodman, M.M., Nelson, S.T., 2020. Using strontium isotopes to trace dust from a drying Great Salt Lake to adjacent urban areas and mountain snowpack. Environ. Res. Lett. 15 (11), 114035.
Chapman, J.B., Ducea, M.N., DeCelles, P.G., Profeta, L., 2015. Tracking changes in crustal thickness during orogenic evolution with Sr/Y: an example from the North American Cordillera. Geology 43 (10), 919–922.
Chen, J.H., Tilton, G.R., 1991. Applications of lead and strontium isotopic relationships to the petrogenesis of granitoid rocks, Central Sierra Nevada batholith, California. Geol. Soc. Am. Bull. 103 (4), 439–447.
Clow, D.W., Mast, M.A., Bullen, T.D., Turk, J.T., 1997. Strontium 87/strontium 86 as a tracer of mineral weathering reactions and calcium sources in an alpine/subalpine watershed, Loch Vale, Colorado. Water Resour. Res. 33 (6), 1335–1351.
Conroy, C.J., Patton, J.L., Lim, M.C., Phuong, M.A., Parmenter, B., Höhna, S., 2016. Following the rivers: historical reconstruction of California voles Microtus californicus (Rodentia: Cricetidae) in the deserts of eastern California. Biol. J. Linn. Soc. 119 (1), 80–98.
Craig, H., 1961. Isotopic variations in meteoric waters. Science 133 (3465), 1702–1703.
Danskin, W.R., 1988. Preliminary Evaluation of the Hydrogeologic System in Owens Valley, California (Vol. 88, No. 4003). Department of the Interior, US Geological Survey.
Danskin, W.R., 1998. Evaluation of the Hydrologic System and Selected Water-Management Alternatives in the Owens Valley, California, vol. 2370. US Geological Survey, Information Services.
Doyle, J.M., Gleeson, T., Manning, A.H., Mayer, K.U., 2015. Using noble gas tracers to constrain a groundwater flow model with recharge elevations: a novel approach for mountainous terrain. Water Resour. Res. 51 (10), 8094–8113.
Dreher, T., 2003. Comment on Güler C, Thyne GD, McCray JE, Turner AK (2002): Evaluation of graphical and multivariate statistical methods for classification of water chemistry data (Hydrogeology Journal 10: 455–474). Hydrogeol. J. 11 (5), 605–606.
Drever, J.I., Zobrist, J., 1992. Chemical weathering of silicate rocks as a function of elevation in the southern Swiss Alps. Geochim. Cosmochim. Acta 56 (8), 3209–3216.
Elder, K., Dozier, J., Michaelsen, J., 1989. Spatial and temporal variation of net snow accumulation in a small alpine watershed, Emerald Lake basin, Sierra Nevada, California, USA. Ann. Glaciol. 13, 56–63.
Feth, J.H.F., Robertson, C.E., Polzer, W.L., 1964. Sources of Mineral Constituents in Water from Granitic Rocks, Sierra Nevada, California and Nevada (No. 1535-I). US Govt. Print. Off.
Forster, C.B., Evans, J.P., 1991. Hydrogeology of thrust faults and crystalline thrust sheets: results of combined field and modeling studies. Geophys. Res. Lett. 18 (5), 979–982.
Friedman, I., Smith, G.I., 1972. Deuterium content of snow as an index to winter climate in the Sierra Nevada Area. Science 176, 790–793.
Friedman, I., Smith, G.I., Johnson, C.A., Moscati, R.J., 2002. Stable isotope compositions of waters in the Great Basin, United States 2. Modern precipitation. J. Geophys. Res.-Atmos. 107 (D19). ACL-15.
Frisbee, M.D., Phillips, F.M., Campbell, A.R., Liu, F., Sanchez, S.A., 2011. Streamflow generation in a large, alpine watershed in the southern Rocky Mountains of Colorado: is streamflow generation simply the aggregation of hillslope runoff responses? Water Resour. Res. 47 (6).
Frisbee, M.D., Phillips, F.M., White, A.F., Campbell, A.R., Liu, F., 2013a. Effect of source integration on the geochemical fluxes from springs. Appl. Geochem. 28, 32–54.
Frisbee, M.D., Wilson, J.L., Gomez-Velez, J.D., Phillips, F.M., Campbell, A.R., 2013b. Are we missing the tail (and the tale) of residence time distributions in watersheds? Geophys. Res. Lett. 40 (17), 4633–4637.
Frisbee, M.D., Meyers, Z.P., Stewart-Maddox, N.S., Caffee, M.W., Bogeholz, P., Hughes, M.N., 2017. What is the source of baseflow in agriculturally fragmented catchments? Complex groundwater/surface-water interactions in three tributary catchments of the Wabash River, Indiana, USA. Hydrol. Process. 31 (22), 4019–4038.
Gardner, W.P., Jencso, K., Hoylman, Z.H., Thiros, N.E., 2018. Mountain Water-The Role of Deep Groundwater in Mountain Watersheds. In AGU Fall Meeting Abstracts. December.
Garrels, R.M., Mackenzie, F.T., 1967. Origin of the Chemical Compositions of some Springs and Lakes.
Gleason, C.L., Frisbee, M.D., Rademacher, L.K., Sada, D.W., Meyers, Z.P., 2020. Hydrogeology of desert springs in the Panamint Range, California, USA: identifying the sources and amount of recharge that support spring flow. Hydrol. Process. 34 (3), 730–748.
Goff, F., Wollenberg, H.A., Brookins, D.C., Kistler, R.W., 1991. A Sr-isotopic comparison between thermal waters, rocks, and hydrothermal calcites, Long Valley caldera, California. J. Volcanol. Geotherm. Res. 48 (3–4), 265–281.
Güler, C., Thyne, G.D., 2004a. Delineation of hydrochemical facies distribution in a regional groundwater system by means of fuzzy c-means clustering. Water Resour. Res. 40 (12).
Güler, C., Thyne, G.D., 2004b. Hydrologic and geologic factors controlling surface and groundwater chemistry in Indian Wells-Owens Valley area, southeastern California, USA. J. Hydrol. 285 (1–4), 177–198.
Guler, C., Thyne, G.D., 2006. Statistical clustering of major solutes: use as a tracer for evaluating interbasin groundwater flow into Indian Wells Valley, California. Environ. Eng. Geosci. 12 (1), 53–65.
Hayashi, M., 2020. Alpine hydrogeology: the critical role of groundwater in sourcing the headwaters of the world. Groundwater 58 (4), 498–510.

Hirt, W.H., 2007. Petrology of the Mount Whitney Intrusive Suite, eastern Sierra Nevada, California: implications for the emplacement and differentiation of composite felsic intrusions. Geol. Soc. Am. Bull. 119 (9–10), 1185–1200.
Hollett, K.J., Danskin, W.R., McCaffrey, W.F., Walti, C.L., 1991. Geology and Water Resources of Owens Valley, California (No. 2370-B), p. USGPO.
Holloway, J.M., Dahlgren, R.A., 2001. Seasonal and event-scale variations in solute chemistry for four Sierra Nevada catchments. J. Hydrol. 250 (1–4), 106–121.
Horton, T.W., Chamberlain, C.P., Fantle, M., Blum, J.D., 1999. Chemical weathering and lithologic controls of water chemistry in a high-elevation river system: Clark's Fork of the Yellowstone River, Wyoming and Montana. Water Resour. Res. 35 (5), 1643–1655.
Jacobson, A.D., Blum, J.D., 2000. Ca/Sr and 87Sr/86Sr geochemistry of disseminated calcite in Himalayan silicate rocks from Nanga Parbat: influence on river-water chemistry. Geology 28 (5), 463–466.
Jacobson, A.D., Blum, J.D., Chamberlain, C.P., Poage, M.A., Sloan, V.F., 2002. Ca/Sr and Sr isotope systematics of a Himalayan glacial chronosequence: carbonate versus silicate weathering rates as a function of landscape surface age. Geochim. Cosmochim. Acta 66 (1), 13–27.
James, E.R., Manga, M., Rose, T.P., Hudson, G.B., 2000. The use of temperature and the isotopes of O, H, C, and noble gases to determine the pattern and spatial extent of groundwater flow. J. Hydrol. 237 (1–2), 100–112.
Jayko, A.S., Bursik, M., 2011. Active transtensional intracontinental basins: Walker Lane in the western Great Basin. Tectonics of sedimentary basins. Rec. Adv. 226–248.
Kahrl, W.L., 1976. The politics of California Water: Owens Valley and the Los Angeles Aqueduct, 1900-1927. Calif. Hist. Q. 55 (1), 2–25.
Kipfer, R., Aeschbach-Hertig, W., Peeters, F., Stute, M., 2002. Noble gases in lakes and ground waters. Rev. Mineral. Geochem. 47 (1), 615–700.
Kistler, R.W., Peterman, Z.E., 1973. Variations in Sr, Rb, K, Na, and initial Sr87/Sr86 in Mesozoic granitic rocks and intruded wall rocks in Central California. Geol. Soc. Am. Bull. 84 (11), 3489–3512.
Liu, Y., Yamanaka, T., 2012. Tracing groundwater recharge sources in a mountain–plain transitional area using stable isotopes and hydrochemistry. J. Hydrol. 464, 116–126.
Lockwood, J.P., Lydon, P.A., 1975. Geologic Map of the Mount Abbot Quadrangle, Central Sierra Nevada. US Geological Survey, California.
Maher, K., 2011. The role of fluid residence time and topographic scales in determining chemical fluxes from landscapes. Earth Planet. Sci. Lett. 312 (1–2), 48–58.
Maher, K., Chamberlain, C.P., 2014. Hydrologic regulation of chemical weathering and the geologic carbon cycle. science 343 (6178), 1502–1504.
Manning, A.H., Solomon, D.K., 2003. Using noble gases to investigate mountain-front recharge. J. Hydrol. 275 (3–4), 194–207.
Manning, A.H., Solomon, D.K., 2005. An integrated environmental tracer approach to characterizing groundwater circulation in a mountain block. Water Resour. Res. 41 (12).
Manning, A.H., Clark, J.F., Diaz, S.H., Rademacher, L.K., Earman, S., Plummer, L.N., 2012. Evolution of groundwater age in a mountain watershed over a period of thirteen years. J. Hydrol. 460, 13–28.
Markovich, K.H., Manning, A.H., Condon, L.E., McIntosh, J.C., 2019. Mountain-block recharge: a review of current understanding. Water Resour. Res. 55 (11), 8278–8304.
Michael, P.J., 1983. Chemical differentiation of the Bishop Tuff and other high-silica magmas through crystallization processes. Geology 11 (1), 31–34.
Miller, J.A., Dunford, A.J., Swana, K.A., Palcsu, L., Butler, M., Clarke, C.E., 2017. Stable isotope and noble gas constraints on the source and residence time of spring water from the Table Mountain Group Aquifer, Paarl, South Africa and implications for large scale abstraction. J. Hydrol. 551, 100–115.
Moore, J.G., 1963. Geology of the Mount Pinchot Quadrangle, Southern Sierra Nevada, California, vol. 1130. US Government Printing Office.
Moore, J.G., 1981. Geologic Map of the Mount Whitney Quadrangle. Inyo and Tulare Counties, California: US Geological Survey Geologic Quadrangle Map GQ-1545, Scale, 1(62,500).
Moore, J.G., 1987. Mount Whitney Quadrangle, Inyo and Tulare Counties, California: Analytic Data (No. 1760). Department of the Interior, US Geological Survey.
Nelson, C.A., 1966. Geologic Map of the Waucoba Mountain Quadrangle. Inyo County, California, vol. 1(62). US Geological Survey Geologic Quadrangle Map GQ-528, p. 500. Scale.
O'Donnell, M.S., Ignizio, D.A., 2012. Bioclimatic predictors for supporting ecological applications in the conterminous United States. US Geol. Surv. Data Ser. 691 (10).
Ormerod, D.S., Rogers, N.W., Hawkesworth, C.J., 1991. Melting in the lithospheric mantle: Inverse modelling of alkali-olivine basalts from the Big Pine Volcanic Field, California. Contrib. Mineral. Petrol. 108 (3), 305–317.
Parkhurst, D.L., Charlton, S.R., 2008. NetpathXL, An Excel Interface to the Program NETPATH (p. 11). US Department of the Interior, US Geological Survey.
Patton, J.L., Conroy, C.J., 2017. The conundrum of subspecies: morphological diversity among desert populations of the California vole (Microtus californicus, Cricetidae). J. Mammal. 98 (4), 1010–1026.
Paukert, A.N., 2014. Mineral Carbonation in Mantle Peridotite of the Samail Ophiolite, Oman: Implications for Permanent Geological Carbon Dioxide Capture and Storage. Doctoral dissertation. Columbia University.
Peeters, F., Beyerle, U., Aeschbach-Hertig, W., Holocher, J., Brennwald, M.S., Kipfer, R., 2003. Improving noble gas based paleoclimate reconstruction and groundwater dating using 20Ne/22Ne ratios. Geochim. Cosmochim. Acta 67 (4), 587–600.
Penman, D.E., Rugenstein, J.K.C., Ibarra, D.E., Winnick, M.J., 2020. Silicate weathering as a feedback and forcing in Earth's climate and carbon cycle. Earth Sci. Rev. 209, 103298.
Peters, E., Visser, A., Esser, B.K., Moran, J.E., 2018. Tracers reveal recharge elevations, groundwater flow paths and travel times on Mount Shasta, California. Water 10 (2), 97.
Plummer, L.N., Prestemon, E.C., Parkhurst, D.L., 1994. An interactive code (NETPATH) for modeling net geochemical reactions along a flow path, version 2.0. Water-Resour. Investig. Rep. 94, 4169.
Pordel, K., 2020. Ecohydrogeology of Owens Valley, California Spring Systems: Relationships between Geochemistry, Benthic Macroinvertebrates, and Microbial Communities. Doctoral dissertation. University of Nevada, Reno.
Pretti, V.A., Stewart, B.W., 2002. Solute sources and chemical weathering in the Owens Lake watershed, eastern California. Water Resour. Res. 38 (8), 2–1.
Rademacher, L.K., Clark, J.F., Hudson, G.B., Erman, D.C., Erman, N.A., 2001. Chemical evolution of shallow groundwater as recorded by springs, Sagehen basin; Nevada County, California. Chem. Geol. 179 (1–4), 37–51.
Rademacher, L.K., Clark, J.F., Clow, D.W., Hudson, G.B., 2005. Old groundwater influence on stream hydrochemistry and catchment response times in a small Sierra Nevada catchment: Sagehen Creek, California. Water Resour. Res. 41 (2).
Reheis, M.C., 1997. Dust deposition downwind of Owens (dry) Lake, 1991–1994: preliminary findings. J. Geophys. Res.-Atmos. 102 (D22), 25999–26008.
Ross, D.C., 1965. Geology of the Independence Quadrangle, Inyo County, California (No. 1181-O). US Govt. Print. Off.
Sada, D., 2008. Great Basin riparian and aquatic ecosystems. In: Chambers, Jeanne C., Devoe, Nora, Evenden, Angela (Eds.), Collaborative Management and Research in the Great Basin-Examining the Issues and Developing a Framework for Action. Gen. Tech. Rep. RMRS-GTR-204. US Department of Agriculture, Forest Service, Rocky Mountain Research Station, Fort Collins, CO, pp. 49–52, 204.
Sada, D.W., Herbst, D.B., 2001. Macroinvertebrates and Environmental Characteristics of Owens Valley Springs, Inyo County, California. Bishop, CA.
Singleton, M.J., Moran, J.E., 2010. Dissolved noble gas and isotopic tracers reveal vulnerability of groundwater in a small, high-elevation catchment to predicted climate changes. Water Resour. Res. 46 (10).
Somers, L.D., McKenzie, J.M., 2020. A review of groundwater in high mountain environments. Wiley Interdiscip. Rev. Water 7 (6), e1475.
Springer, A.E., Stevens, L.E., 2009. Spheres of discharge of springs. Hydrogeol. J. 17 (1), 83.
Stone, P., Dunne, G.C., Moore, J.G., Smith, G.I., 2000. Geologic Map of the Lone Pine 15′ Quadrangle, Inyo County. The Survey, California.
Taylor, T.R., Dewey, J.F., 2009. Transtensional analyses of fault patterns and strain provinces of the Eastern California shear zone–Walker Lane on the eastern margin of the Sierra Nevada microplate, California and Nevada. Int. Geol. Rev. 51 (9–11), 843–872.
Thomas, J.M., Hudson, B.G., Stute, M., Clark, J.F., 2003. Noble gas loss may indicate groundwater flow across flow barriers in southern Nevada. Environ. Geol. 43 (5), 568–579.
Wesnousky, S.G., 2005. The San Andreas and Walker Lane fault systems, western North America: Transpression, transtension, cumulative slip and the structural evolution of a major transform plate boundary. J. Struct. Geol. 27 (8), 1505–1512.
White, A.F., Bullen, T.D., Vivit, D.V., Schulz, M.S., Clow, D.W., 1999. The role of disseminated calcite in the chemical weathering of granitoid rocks. Geochim. Cosmochim. Acta 63 (13–14), 1939–1953.
White, A.F., Schulz, M.S., Lowenstern, J.B., Vivit, D.V., Bullen, T.D., 2005. The ubiquitous nature of accessory calcite in granitoid rocks: implications for weathering, solute evolution, and petrogenesis. Geochim. Cosmochim. Acta 69 (6), 1455–1471.
Williams, M.W., Melack, J.M., 1991. Solute chemistry of snowmelt and runoff in an alpine basin, Sierra Nevada. Water Resour. Res. 27 (7), 1575–1588.
Wilson, J.L., Guan, H., 2004. Mountain-Block Hydrology and Mountain-Front Recharge. Groundwater Recharge in a Desert Environment. The Southwestern United States, p. 9.
Winnick, M.J., Maher, K., 2018. Relationships between CO2, thermodynamic limits on silicate weathering, and the strength of the silicate weathering feedback. Earth Planet. Sci. Lett. 485, 111–120.
Zhang, A., 2021. Delineation of spring capture zones in southern Great Basin, USA based on modeling results and geochemical data. Water Sci. Eng. In press.
Zheng, Z., Kirchner, P.B., Bales, R.C., 2016. Topographic and vegetation effects on snow accumulation in the southern Sierra Nevada: a statistical summary from lidar data. Cryosphere 10 (1), 257–269.
Zuber, A., Weise, S.M., Osenbrück, K., Grabczak, J., Ciężkowski, W., 1995. Age and recharge area of thermal waters in Ladek Spa (Sudeten, Poland) deduced from environmental isotope and noble gas data. J. Hydrol. 167 (1–4), 327–349.